

**Figure 5** Effect of bone marrow transplanted (BMT) using bone marrow from young animals into aged animals on the density of vascular structures in the periinfarction area during the poststroke period. (A–C) Representative micrographs of cerebral cortex about 0.5 mm from the stroke-affected area in the phosphate-buffered saline (PBS) (A) and BMT (B) groups on day 30 after stroke. Sections were stained with anti-Lectin antibody. There is a significant difference in vascular density observed between groups (C). (D–F) Representative micrographs of contralateral cortex in the PBS (D) and BMT (E) groups on day 30 after stroke. No significant difference in vascular density was observed between the two groups (F). (G–J) Representative micrograph of ipsilateral stroke-affected cortex (G) and contralateral cortex (I) of a poststroke young rat on day 30 after stroke. Compared with aged rats subjected to stroke, there is a significant increase in vascular density in the stroke-affected cortex located about 0.5 mm from the stroke area (H) and contralateral cortex (J) in the young animals. (K) Human umbilical vein endothelial cells (HUVECs) were exposed to bone marrow mononuclear cells from aged or young rats and the level of endothelial cell phospho-p38 was determined. Analysis of variance analysis revealed a significant reduction in endothelial phospho-p38 in the presence of young bone marrow cells compared with aged bone marrow cells. (L–N) Representative micrographs of cerebral cortex about 0.5 mm from the stroke-affected area from an animal in the PBS (L) and BMT (M) group on day 30 after stroke. The section is stained with anti-Iba-1 antibody. A significant reduction in microglia was observed in the BMT group, compared with PBS-treated group (N). \* $P < 0.05$  versus PBS control (C, N) or aged bone marrow (H, J, K).  $n = 5$ , in each group. Scale bar: 50  $\mu$ m (A, L).

bone marrow into aged animals are not likely due to modulating the profile of inflammatory cytokines at the site of cerebral infarction or in the serum.

Vascular endothelial dysfunction in aging has been shown to be correlate with impaired vasodilatation (LeBlanc *et al*, 2008) and reduced expression of NOS

(Smith and Hagen, 2003). Although some aspects of cell senescence are likely to be irreversible, certain endothelial properties can be maintained/restored with antioxidants (Smith and Hagen, 2003). Furthermore, exposure to a 'young systemic environment' has been shown to rejuvenate aged progenitor cells in rats (Conboy et al, 2005). Taken together with these previous observations, our results indicate that partial reconstitution of bone marrow from aged rats with cells from young animals improves the host response to cerebral ischemia, probably in part through a beneficial effect on endothelial function. Although bone marrow cells have the potential to differentiate into endothelial cells (Asahara et al, 1997), the half-life of endothelial cells is relatively long and differentiation of circulating cells into endothelium is relatively rare (Taguchi et al, 2004b). Thus, the principal effect of young progenitors in the bone marrow may be to promote an environment in the systemic circulation conducive to vascular activation, as evidenced by increased levels of phospho-eNOS (i.e., the results of our *in vitro* studies with cultured HUVEC exposed to mononuclear bone marrow cells from young versus old rats; Figure 4E). In addition to eNOS, young bone marrow cells were shown to decrease activation of p38 MAP kinase in cultured endothelium, a pathway leading to cell death (Mehta et al, 2007). In contrast, no significant change in activation/inactivation of other MAP kinases, ERK1/2 or JNK, was observed in endothelial cells exposed to bone marrow cells from young animals *in vitro*. In a previous report, inactivation of p38, but not JNK, was shown to suppress endothelial cell death after hypoxia/reoxygenation injury (Lee and Lo, 2003). Taken together, our data thus far suggests that the beneficial effect of bone marrow cells from young animals may be due, at least in part, to effects on the vascular endothelium, especially at the level of cerebral microvasculature. This concept is consistent with our observation of an increased density of vascular structures in the periinfarct area of poststroke brain from aged rats transplanted with bone marrow cells from young animals. However, the precise mechanisms linking bone marrow-derived immature cells to enhanced function of the cerebral microcirculation remains to be determined (Pearson, 2009). In view of the likely impact of inflammatory mechanisms on reparative mechanisms in stroke, another important observation might be the decrease of microglial invasion/activation observed in poststroke aged animals transplanted with bone marrow from young animals.

Our results suggest a novel strategy for enhancing the host response to ischemia in aged patients, provided these observations in a rodent model can be translated to humans. If such an extrapolation to man is possible, the source of 'young' bone marrow is relatively easily obtained through collection and preservation of autologous cord blood or bone marrow cells harvested earlier in life. In addition,

an alternative approach might be induction of hematopoietic stem cells using autologous induced pluripotent stem (iPS) cells (Hanna et al, 2007). Although the fundamental mechanisms underlying senescence of mammalian cells (and senescence of the vasculature) remains to be elucidated, our findings indicate that impairment of the vascular response in aged individuals may be partially restored through transplantation with bone marrow from young animals. In addition to possible therapeutic application in patients with an evolving stroke, rejuvenation of bone marrow may also have a preventive role in those at high risk for stroke, such as individuals with recurrent transient ischemic attacks.

## Disclosure/conflict of interest

The authors declare no conflict of interest.

## References

Asahara T, Murohara T, Sullivan A, Silver M, van der Zee R, Li T, Witzenbichler B, Schatteman G, Isner JM (1997) Isolation of putative progenitor endothelial cells for angiogenesis. *Science* 275:964–7

Brandle M, al Makdessi S, Weber RK, Dietz K, Jacob R (1997) Prolongation of life span in hypertensive rats by dietary interventions. Effects of garlic and linseed oil. *Basic Res Cardiol* 92:223–32

Chen Y, Hallenbeck JM, Ruetzler C, Bol D, Thomas K, Berman NE, Vogel SN (2003) Overexpression of monocyte chemoattractant protein 1 in the brain exacerbates ischemic brain injury and is associated with recruitment of inflammatory cells. *J Cereb Blood Flow Metab* 23: 748–55

Conboy IM, Conboy MJ, Wagers AJ, Girma ER, Weissman IL, Rando TA (2005) Rejuvenation of aged progenitor cells by exposure to a young systemic environment. *Nature* 433:760–4

Farkas T, Racekova E, Kis Z, Horvath S, Burda J, Galik J, Toldi J (2003) Peripheral nerve injury influences the disinhibition induced by focal ischaemia in the rat motor cortex. *Neurosci Lett* 342:49–52

Hanna J, Wernig M, Markoulaki S, Sun CW, Meissner A, Cassady JP, Beard C, Brambrink T, Wu LC, Townes TM, Jaenisch R (2007) Treatment of sickle cell anemia mouse model with iPS cells generated from autologous skin. *Science* 318:1920–3

Hill JM, Zalos G, Halcox JP, Schenke WH, Waclawiw MA, Quyyumi AA, Finkel T (2003) Circulating endothelial progenitor cells, vascular function, and cardiovascular risk. *N Engl J Med* 348:593–600

Holmin S, Mathiesen T (2000) Intracerebral administration of interleukin-1beta and induction of inflammation, apoptosis, and vasogenic edema. *J Neurosurg* 92:108–20

Hutchins PM, Lynch CD, Cooney PT, Curseen KA (1996) The microcirculation in experimental hypertension and aging. *Cardiovasc Res* 32:772–80

Inaba M, Adachi Y, Hisha H, Hosaka N, Maki M, Ueda Y, Koike Y, Miyake T, Fukui J, Cui Y, Mukai H, Koike N, Omae M, Mizokami T, Shigematsu A, Sakaguchi Y, Tsuda M, Okazaki S, Wang X, Li Q, Nishida A, Ando Y, Guo K, Song C, Cui W, Feng W, Katou J, Sado K, Nakamura S, Ikehara S (2007) Extensive studies on

perfusion method plus intra-bone marrow-bone marrow transplantation using cynomolgus monkeys. *Stem Cells* 25:2098–103

Kamihata H, Matsubara H, Nishie T, Fujiyama S, Tsutsumi Y, Ozono R, Masaki H, Mori Y, Iba O, Tateishi E, Kosaki A, Shintani S, Murohara T, Imaizumi T, Iwasaka T (2001) Implantation of bone marrow mononuclear cells into ischemic myocardium enhances collateral perfusion and regional function via side supply of angioblasts, angiogenic ligands, and cytokines. *Circulation* 104:1046–52

Kant S, Schumacher S, Singh MK, Kispert A, Kotlyarov A, Gaestel M (2006) Characterization of the atypical MAPK ERK4 and its activation of the MAPK-activated protein kinase MK5. *J Biol Chem* 281:35511–9

Kasahara Y, Taguchi A, Uno H, Nakano A, Nakagomi T, Hirose H, Stern DM, Matsuyama T (2010) Telmisartan suppresses cerebral injury in a murine model of transient focal ischemia. *Brain Res* 1340:70–80

LeBlanc AJ, Shipley RD, Kang LS, Muller-Delp JM (2008) Age impairs Flk-1 signaling and NO-mediated vasodilation in coronary arterioles. *Am J Physiol Heart Circ Physiol* 295:H2280–8

Lee SR, Lo EH (2003) Interactions between p38 mitogen-activated protein kinase and caspase-3 in cerebral endothelial cell death after hypoxia-reoxygenation. *Stroke* 34:2704–9

Li C, He Y, Feng X, Inaba M, Adachi Y, Takada K, Zhang Y, Yamamoto Y, Wu X, Cui Y, Iwasaki M, Hisha H, Hosaka N, Taira M, Minamino K, Suzuki Y, Nakano K, Fukui J, Ueda Y, Koike Y, Tsuda M, Ikehara S (2007) An innovative approach to bone marrow collection and transplantation in a patient with beta-thalassemia major: marrow collection using a perfusion method followed by intra-bone marrow injection of collected bone marrow cells. *Int J Hematol* 85:73–7

Loddick SA, Turnbull AV, Rothwell NJ (1998) Cerebral interleukin-6 is neuroprotective during permanent focal cerebral ischemia in the rat. *J Cereb Blood Flow Metab* 18:176–9

Lynch CD, Cooney PT, Bennett SA, Thornton PL, Khan AS, Ingram RL, Sonntag WE (1999) Effects of moderate caloric restriction on cortical microvascular density and local cerebral blood flow in aged rats. *Neurobiol Aging* 20:191–200

Majka M, Janowska-Wieczorek A, Ratajczak J, Ehrenman K, Pietrzkowski Z, Kowalska MA, Gewirtz AM, Emerson SG, Ratajczak MZ (2001) Numerous growth factors, cytokines, and chemokines are secreted by human CD34(+) cells, myeloblasts, erythroblasts, and megakaryoblasts and regulate normal hematopoiesis in an autocrine/paracrine manner. *Blood* 97:3075–85

Meaney MJ, O'Donnell D, Rowe W, Tannenbaum B, Steverman A, Walker M, Nair NP, Lupien S (1995) Individual differences in hypothalamic-pituitary-adrenal activity in later life and hippocampal aging. *Exp Gerontol* 30:229–51

Mehta SL, Manhas N, Raghbir R (2007) Molecular targets in cerebral ischemia for developing novel therapeutics. *Brain Res Rev* 54:34–66

Pearce DJ, Anjos-Afonso F, Ridder CM, Eddaoudi A, Bonnet D (2007) Age-dependent increase in side population distribution within hematopoiesis: implications for our understanding of the mechanism of aging. *Stem Cells* 25:828–35

Pearson JD (2009) Endothelial progenitor cells—hype or hope? *J Thromb Haemost* 7:255–62

Schmidt-Lucke C, Rossig L, Fichtlscherer S, Vasa M, Britten M, Kamper U, Dimmeler S, Zeiher AM (2005) Reduced number of circulating endothelial progenitor cells predicts future cardiovascular events: proof of concept for the clinical importance of endogenous vascular repair. *Circulation* 111:2981–7

Smith AR, Hagen TM (2003) Vascular endothelial dysfunction in aging: loss of Akt-dependent endothelial nitric oxide synthase phosphorylation and partial restoration by (R)-alpha-lipoic acid. *Biochem Soc Trans* 31:1447–9

Sonntag WE, Lynch CD, Cooney PT, Hutchins PM (1997) Decreases in cerebral microvasculature with age are associated with the decline in growth hormone and insulin-like growth factor 1. *Endocrinology* 138:3515–20

Sullivan PG, Bruce-Keller AJ, Rabchevsky AG, Christakos S, Clair DK, Mattson MP, Scheff SW (1999) Exacerbation of damage and altered NF- $\kappa$ B activation in mice lacking tumor necrosis factor receptors after traumatic brain injury. *J Neurosci* 19:6248–56

Taguchi A (2009) Vascular factors in diabetes and Alzheimer's disease. *J Alzheimers Dis* 16:859–64

Taguchi A, Matsuyama T, Moriwaki H, Hayashi T, Hayashida K, Nagatsuka K, Todo K, Mori K, Stern DM, Soma T, Naritomi H (2004a) Circulating CD34-positive cells provide an index of cerebrovascular function. *Circulation* 109:2972–5

Taguchi A, Matsuyama T, Nakagomi T, Shimizu Y, Fukunaga R, Tatsumi Y, Yoshikawa H, Kikuchi-Taura A, Soma T, Moriwaki H, Nagatsuka K, Stern DM, Naritomi H (2008) Circulating CD34-positive cells provide a marker of vascular risk associated with cognitive impairment. *J Cereb Blood Flow Metab* 28:445–9

Taguchi A, Nakagomi N, Matsuyama T, Kikuchi-Taura A, Yoshikawa H, Kasahara Y, Hirose H, Moriwaki H, Nakagomi T, Soma T, Stern DM, Naritomi H (2009) Circulating CD34-positive cells have prognostic value for neurologic function in patients with past cerebral infarction. *J Cereb Blood Flow Metab* 29:34–8

Taguchi A, Ohtani M, Soma T, Watanabe M, Kinoshita N (2003) Therapeutic angiogenesis by autologous bone-marrow transplantation in a general hospital setting. *Eur J Vasc Endovasc Surg* 25:276–8

Taguchi A, Soma T, Tanaka H, Kanda T, Nishimura H, Yoshikawa H, Tsukamoto Y, Iso H, Fujimori Y, Stern DM, Naritomi H, Matsuyama T (2004b) Administration of CD34+ cells after stroke enhances neurogenesis via angiogenesis in a mouse model. *J Clin Invest* 114:330–8

Taguchi A, Wen Z, Myojin K, Yoshihara T, Nakagomi T, Nakayama D, Tanaka H, Soma T, Stern DM, Naritomi H, Matsuyama T (2007) Granulocyte colony-stimulating factor has a negative effect on stroke outcome in a murine model. *Eur J Neurosci* 26:126–33

Tateishi-Yuyama E, Matsubara H, Murohara T, Ikeda U, Shintani S, Masaki H, Amano K, Kishimoto Y, Yoshimoto K, Akashi H, Shimada K, Iwasaka T, Imaizumi T (2002) Therapeutic angiogenesis for patients with limb ischaemia by autologous transplantation of bone-marrow cells: a pilot study and a randomised controlled trial. *Lancet* 360:427–35

Watson JV, Nakeff A, Chambers SH, Smith PJ (1985) Flow cytometric fluorescence emission spectrum analysis of Hoechst-33342-stained DNA in chicken thymocytes. *Cytometry* 6:310–5

Werner N, Kosiol S, Schiegl T, Ahlers P, Walenta K, Link A, Bohm M, Nickenig G (2005) Circulating endothelial

progenitor cells and cardiovascular outcomes. *N Engl J Med* 353:999–1007

Yamahara K, Sone M, Itoh H, Yamashita JK, Yurugi-Kobayashi T, Homma K, Chao TH, Miyashita K, Park K, Oyamada N, Sawada N, Taura D, Fukunaga Y, Tamura N, Nakao K (2008) Augmentation of neovascularization in hindlimb ischemia by combined transplantation of human embryonic stem cells-derived endothelial and mural cells. *PLoS One* 3:e1666

Yang GY, Gong C, Qin Z, Ye W, Mao Y, Bertz AL (1998) Inhibition of TNFalpha attenuates infarct volume and ICAM-1 expression in ischemic mouse brain. *Neuroreport* 9:2131–4

Yoshihara T, Taguchi A, Matsuyama T, Shimizu Y, Kikuchi-Taura A, Soma T, Stern DM, Yoshikawa H, Kasahara Y, Moriwaki H, Nagatsuka K, Naritomi H (2008) Increase in circulating CD34-positive cells in patients with angiographic evidence of moyamoya-like vessels. *J Cereb Blood Flow Metab* 28:1086–9

Zhang B, Hata R, Zhu P, Sato K, Wen TC, Yang L, Fujita H, Mitsuda N, Tanaka J, Samukawa K, Maeda N, Sakanaka M (2006) Prevention of ischemic neuronal death by intravenous infusion of a ginseng saponin, ginsenoside Rb(1), that upregulates Bcl-x(L) expression. *J Cereb Blood Flow Metab* 26:708–21



This work is licensed under the Creative Commons Attribution-NonCommercial-No Derivative Works 3.0 Unported License. To view a copy of this license, visit <http://creativecommons.org/licenses/by-nc-nd/3.0/>

# Quantification of regional myocardial oxygen metabolism in normal pigs using positron emission tomography with injectable $^{15}\text{O-O}_2$

Takashi Temma · Hidehiro Iida · Takuya Hayashi · Noboru Teramoto · Youichiro Ohta · Nobuyuki Kudomi · Hiroshi Watabe · Hideo Saji · Yasuhiro Magata

Received: 27 April 2009 / Accepted: 10 August 2009 / Published online: 4 September 2009  
© Springer-Verlag 2009

## Abstract

**Purpose** Although  $^{15}\text{O-O}_2$  gas inhalation can provide a reliable and accurate myocardial metabolic rate for oxygen by PET, the spillover from gas volume in the lung distorts the images. Recently, we developed an injectable method in which blood takes up  $^{15}\text{O-O}_2$  from an artificial lung, and this made it possible to estimate oxygen metabolism without the inhalation protocol. In the present study, we evaluated the effectiveness of the injectable  $^{15}\text{O-O}_2$  system in porcine hearts.

**Methods** PET scans were performed after bolus injection and continuous infusion of injectable  $^{15}\text{O-O}_2$  via a shunt between the femoral artery and the vein in normal pigs. The injection method was compared to the inhalation method. The oxygen extraction fraction (OEF) in the lateral walls of the heart was calculated by a compartmental model in view of the spillover and partial volume effect.

**Results** A significant decrease of lung radioactivity in PET images was observed compared to the continuous inhalation

of  $^{15}\text{O-O}_2$  gas. Furthermore, the injectable  $^{15}\text{O-O}_2$  system provides a measurement of OEF in lateral walls of the heart that is similar to the continuous-inhalation method ( $0.71 \pm 0.036$  and  $0.72 \pm 0.020$  for the bolus-injection and continuous-infusion methods, respectively).

**Conclusion** These results indicate that injectable  $^{15}\text{O-O}_2$  has the potential to evaluate myocardial oxygen metabolism.

**Keywords** Myocardial oxygen metabolism · PET · Pig · OEF · Injectables  $^{15}\text{O-O}_2$

## Introduction

In the myocardium, fatty acid or glucose is used to produce energy by aerobic metabolism. Oxygen is one of the most important substrates closely related to the aerobic metabolism in the TCA cycle; thus, oxygen metabolism should be a direct reflection of myocardial metabolism of these substrates. Therefore, there has been considerable interest in the development of a method to quantify oxygen metabolism in the myocardium.

Recently,  $^{11}\text{C}$ -acetate has been used for this purpose [1–5].  $^{11}\text{C}$ -acetate is taken up by the mitochondria and metabolically converted into acetyl-CoA. It then enters the TCA cycle and is transformed to  $^{11}\text{C-CO}_2$ , which is cleared rapidly from the myocardium. Thus, the clearance pharmacokinetics reflects oxygen metabolism in the myocardium. However, the quantification of oxygen metabolism using  $^{11}\text{C}$ -acetate is quite difficult because of various intermediary compounds.

The use of  $^{15}\text{O-O}_2$  gas inhalation and PET scanning can provide a quantitative myocardial metabolic rate for oxygen (MMRO<sub>2</sub>) [6, 7]. The tracer kinetic model used is based on that originally proposed to describe the behavior of  $^{15}\text{O-O}_2$  in brain tissue [8, 9]. However, the direct translation of the

T. Temma · H. Saji  
Department of Patho-Functional Bioanalysis,  
Graduate School of Pharmaceutical Sciences, Kyoto University,  
Kyoto, Japan

H. Iida · T. Hayashi · N. Teramoto · Y. Ohta · N. Kudomi ·  
H. Watabe  
Department of Investigative Radiology,  
National Cardiovascular Center Research Institute,  
Osaka, Japan

Y. Magata (✉)  
Laboratory of Genome Bio-Photonics,  
Photon Medical Research Center,  
Hamamatsu University School of Medicine,  
1-20-1 Handayama,  
Hamamatsu 431-3192, Japan  
e-mail: magata@hama-med.ac.jp

compartmental model for the brain to the heart is not permitted, because subtraction for spillover from gas volume in addition to that from the blood pool is needed. A previous study demonstrated that the gas volume can be accurately estimated from the transmission scan data; thus, this technique did not require additional emission scanning for estimating the quantitative gas volume images [6, 7]. However, gaseous radioactivity in the lung during the inhalation of  $^{15}\text{O}$ -O<sub>2</sub> gas is too high in comparison to other regions. Subtraction for this contribution is straightforward and accurate using the transmission scan-derived gaseous volume images, but the lung radioactivity degraded image quality in the estimated MMRO<sub>2</sub> images.

As an alternative to gas inhalation, we recently developed a method to prepare an injectable form of  $^{15}\text{O}$ -O<sub>2</sub>. This was accomplished by exposing pre-collected blood to  $^{15}\text{O}$ -O<sub>2</sub> gas using a small artificial lung system resulting in a maximum yield of 130 MBq/ml. We demonstrated that cerebral oxygen metabolism could be estimated in normal and ischemic rats using injectable  $^{15}\text{O}$ -O<sub>2</sub> [10–12]. This technique has the potential of avoiding the inhalation protocol.

The aim of the present study was therefore to test the feasibility of using the injectable  $^{15}\text{O}$ -O<sub>2</sub> oxygen system for estimating myocardial oxygen metabolism in pigs. The injection method was compared to the inhalation method to determine if the injection method resulted in a reduction of lung radioactivity, an improved image quality, a more accurate estimate of myocardial oxygen metabolism, and an improved signal-to-noise ratio.

## Materials and methods

### Theory

$^{15}\text{O}$ -Oxygen was administered by IV injection or inhalation and was carried as  $^{15}\text{O}$ -hemoglobin by blood to peripheral tissues including the myocardium, where it was converted to  $^{15}\text{O}$ -water ( $^{15}\text{O}$ -H<sub>2</sub>O<sub>met</sub>) through aerobic metabolism. The increased distribution volume of  $^{15}\text{O}$ -H<sub>2</sub>O<sub>met</sub>, represented by the exchangeable water space of tissue, causes delayed removal of radioactivity. This allows the definition of an appropriate model and equations to be derived for the calculation of a regional myocardial metabolic rate for oxygen (rMMOR<sub>2</sub>) and regional oxygen extraction fraction (rOEF). Previous studies demonstrated that these calculations were similar to those used for estimating cerebral blood flow and oxygen metabolism and require the measurement of regional myocardial blood flow (rMBF) and a correction for spillover of activity from the vascular pools and the pulmonary alveoli [6, 7]. rMBF was measured by the  $^{15}\text{O}$ -H<sub>2</sub>O injection technique [13]. Activity in the vascular

pools of the heart chambers and the lung was evaluated with a conventional measurement of blood volume using  $^{15}\text{O}$ -CO, and activity in the pulmonary alveoli was evaluated with an unconventional and indirect measurement of gas volume obtained from the transmission scan. Furthermore, the existence of recirculating  $^{15}\text{O}$ -H<sub>2</sub>O<sub>met</sub> in the blood freely accessible to the myocardium was taken into consideration.

The differential equation describing the myocardial kinetics after administration of  $^{15}\text{O}$ -O<sub>2</sub> can be written as follows:

$$\frac{dC^{\text{myo}}(t)}{dt} = \text{OEF} \cdot f \cdot A_o(t) + f \cdot A_w(t) - \left( \frac{f}{p} + \lambda \right) C^{\text{myo}}(t) \quad (1)$$

where  $C^{\text{myo}}(t)$  designates the true radioactivity concentration in the myocardium at time  $t$ ,  $f$  is myocardial blood flow,  $A_o(t)$  is the  $^{15}\text{O}$ -O<sub>2</sub> radioactivity concentration in arterial blood,  $A_w(t)$  is the  $^{15}\text{O}$ -H<sub>2</sub>O radioactivity concentration in arterial blood,  $p$  is the myocardium/blood partition coefficient of water, and  $\lambda$  is the physical decay constant of O-15.

Solving Eq. (1) in terms of  $C^{\text{myo}}(t)$  gives:

$$C^{\text{myo}}(t) = \text{OEF} \cdot f \cdot A_o(t) * e^{-(\frac{f}{p} + \lambda) \cdot t} + f \cdot A_w(t) * e^{-(\frac{f}{p} + \lambda) \cdot t} \quad (2)$$

where the asterisk denotes the convolution integral. During steady-state conditions under the continuous administration of  $^{15}\text{O}$ -O<sub>2</sub>, the following relationship holds:

$$C^{\text{myo}} = \frac{\text{OEF} \cdot f \cdot A_o + f \cdot A_w}{\left( \frac{f}{p} + \lambda \right)} \quad (3)$$

In the actual PET studies, the spillover from vascular pools and pulmonary alveoli and the partial volume effect should be taken into consideration [14]. Then, the measured radioactivity concentration in the region of interest (ROI) in the myocardium ( $R^{\text{myo}}(t)$ ) can be expressed as:

$$R^{\text{myo}}(t) = \alpha \cdot C^{\text{myo}}(t) + (V_B^{\text{myo}} \cdot A_t(t) - \alpha \cdot F_{\text{vein}} \cdot \text{OEF} \cdot A_o(t) - \alpha \cdot F_{\text{vein}} \cdot A_w(t)) + V_G^{\text{myo}} \cdot C_{\text{gas}}(t) \quad (4)$$

where  $\alpha$  denotes the myocardial tissue fraction,  $V_B^{\text{myo}}$  is the myocardial blood volume,  $A_t(t)$  is the total O-15 radioactivity concentration in arterial blood,  $F_{\text{vein}}$  is the microscopic venous blood volume,  $V_G^{\text{myo}}$  is the gas volume in the myocardial ROI and  $C_{\text{gas}}(t)$  is the O-15 radioactivity concentration in  $V_G^{\text{myo}}$ .

With the bolus injection or infusion methods using an artificial lung system, the radioactivity in the pulmonary alveoli is expected to be negligible in comparison with the inhalation method. Thus, Eq. (4) can be converted to:

$$R^{\text{myo}}(t) = \alpha \cdot C^{\text{myo}}(t) + (V_B^{\text{myo}} \cdot A_t(t) - \alpha \cdot F_{\text{vein}} \cdot OEF \cdot A_o(t) - \alpha \cdot F_{\text{vein}} \cdot A_w(t)) \quad (5)$$

## Subjects

In this study, four healthy miniature pigs (22–30 kg) were used. The pigs were anesthetized by IM injection of ketamine and xylazine followed by continuous infusion of propofol (5 mg/kg/h). The animals were then placed in the supine position on the bed of the PET scanner. All experimental procedures were approved by the local animal welfare committee.

## Injectable $^{15}\text{O}$ -O<sub>2</sub> preparation

In the “injection” study, injectable  $^{15}\text{O}$ -O<sub>2</sub> was used. Injectable  $^{15}\text{O}$ -O<sub>2</sub> was prepared as described previously [10–12]. In brief, part of an infusion line kit (Terumo Corporation, Tokyo, Japan) and an artificial lung 18 cm in length (Senko Medical Instrument Mfg Co. Ltd., Tokyo, Japan) were connected using silicone tubing to make a closed system. Then, venous blood collected from a pig, which was used in the following PET studies, was added to the system and circulated (100 ml/min) by a peristaltic pump, followed by introduction of  $^{15}\text{O}$ -O<sub>2</sub> gas (~7,000 MBq/min/433 ml) into the artificial lung for 15 min to prepare injectable  $^{15}\text{O}$ -O<sub>2</sub> (5.6–60.7 MBq/ml).

In the “continuous infusion” study, the left femoral artery and right femoral vein were both cannulated. The two cannulas from the artery and the vein were connected to the opposite sides of an artificial lung to create a femoral shunt. The blood flow in the shunt was aided by a peristaltic pump (30–50 ml/min).  $^{15}\text{O}$ -O<sub>2</sub> gas (~7,000 MBq/min/433 ml) was continuously introduced into the artificial lung.

## PET protocol (Fig. 1)

The PET scanner was an ECAT EXACT HR (CTI/Siemens) [15], which has an imaging field of view (FOV) of 55 cm in diameter and 15 cm in axial length. The spatial resolution of the scanner is 5.8 mm in full width at half maximum at the center of the FOV.

After obtaining a 20-min transmission scan for attenuation correction and gas volume estimation, the blood pool image was obtained with a 4-min PET scan after the pigs inhaled 2.7 GBq  $^{15}\text{O}$ -CO for 30 s. Arterial blood samples were taken every minute during the  $^{15}\text{O}$ -CO scanning, and

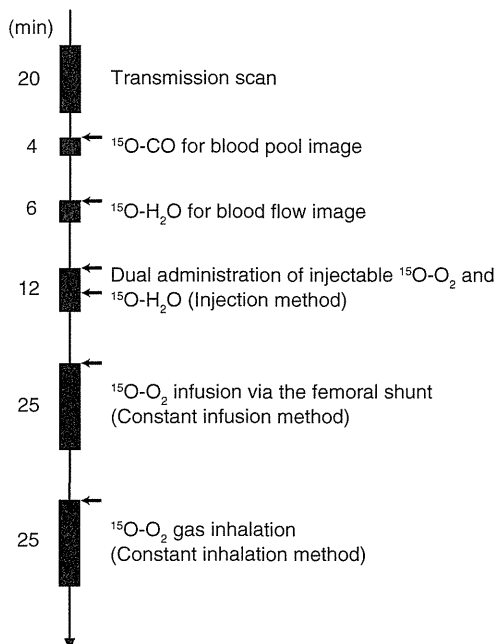


**Fig. 1** Outline of the PET imaging study. The interval between scans was more than 15 min to allow for physical decay of O-15 radioactivity to background levels

the radioactivity concentration in the whole blood was measured with a NaI well-type scintillation counter calibrated against the PET scanner. Subsequently,  $^{15}\text{O}$ -water was injected into the right femoral vein for 30 s at an infusion rate of 10 ml/min (injected radioactivity was about 1.11 GBq). Immediately after injection of  $^{15}\text{O}$ -water, 26 dynamic frames (12×5 s, 8×15 s and 6×30 s) of PET data were acquired for 6 min.

Furthermore, two PET scans were successively performed after the IV injection of  $^{15}\text{O}$ -O<sub>2</sub> (5.6–60.7 MBq/ml) for 30 s at an injection rate of 20–80 ml/min for the “injection” study, and by the continuous  $^{15}\text{O}$ -O<sub>2</sub> gas infusion through the artificial lung in the femoral shunt for the “continuous infusion” study. In the “injection” study, 52 dynamic frames (12×5 s, 8×15 s, 6×30 s, 12×5 s, 8×15 s and 6×30 s) of PET data were acquired for 12 min, and 1.11 GBq of  $^{15}\text{O}$ -water was injected IV for 30 s at 10 ml/min starting at 6 min after the administration of IV  $^{15}\text{O}$ -O<sub>2</sub> according to the dual administration protocol we developed previously [16]. In the “continuous infusion” study, 26 dynamic frames (10×30 s, 5×60 s, 1×600 s and 10×30 s) were acquired for 25 min, and the 600-s frame was used for steady-state analysis.

Another PET scan was performed by  $^{15}\text{O}$ -O<sub>2</sub> gas inhalation in one of the four pigs in the same protocol as the “continuous infusion” study. This was the “continuous inhalation” study. The interval between scans was more

than 15 min to allow for physical decay of  $^{15}\text{O}$ -radioactivity to background levels. All acquisitions were obtained in the two-dimensional mode (septa extended).

#### Data analysis

A filtered back-projection algorithm with a 6-mm Gaussian filter was used for image reconstruction. The reconstructed images had a matrix size of  $128 \times 128 \times 47$  and a voxel size of  $1.84 \times 1.84 \times 3.38$  mm, and all image data sets were resliced into short-axis images across the left ventricle [13].

#### Myocardial blood flow

rMBF was calculated from the injection of  $^{15}\text{O}$ -H<sub>2</sub>O by fitting the myocardial and arterial time-activity curve data to a single-tissue-compartment model that implemented corrections for partial-volume effects by introducing the tissue fraction. In addition, the model was corrected for spillover from the left ventricular (LV) chamber into the myocardial ROI by introducing the arterial blood volume [13]. In these experiments, the time-activity curves generated from large ROIs placed in the LV chamber were used as the input function.

#### Regional oxygen extraction fraction

In the “injection” study, rOEF was calculated according to Eqs. (2) and (5). In these formulations,  $F_{\text{vein}}$  was assumed to be 0.10 ml/g tissue and  $p$  was fixed at 0.90 ml/g. The blood volume image obtained from the  $^{15}\text{O}$ -CO scan was used for the determination of  $V_B^{\text{myo}}$ . The value of  $A_t(t)$  was obtained from the LV radioactivity concentration measured from the PET data set with small LV ROIs to minimize spillover from the myocardium. The calculation for the estimation of recirculating  $^{15}\text{O}$ -H<sub>2</sub>O was performed as previously described [16]. For the “continuous infusion” and “continuous inhalation” studies, in which a 600-s frame was regarded as steady-state, Eqs. (3) and (5) or Eqs. (3) and (4) were used for calculating rOEF, respectively.

## Results

Table 1 summarizes the conditions of animals during the PET studies. The parameters were all within the physiologic range.

**Table 1** Physiological parameters of pigs during the PET studies

	pH	pCO <sub>2</sub> (mmHg)	pO <sub>2</sub> (mmHg)	tHb (g/dl)	O <sub>2</sub> Sat (%)	HR (bpm)	BP (mmHg)	
							Diastolic	Systolic
Average	7.46	40.3	125.8	12.8	97.7	85	97.8	125.2
SD	0.032	2.51	16.69	1.30	1.83	19.5	10.4	19.3

Figure 2 demonstrates the dynamic images obtained in the “injection”, “continuous infusion”, and “continuous inhalation” studies. With the injection and continuous-infusion methods, the right ventricle on the left side and the vena cava on the lower side were well delineated, whereas the left ventricle was moderately shown on the right side. The 16th frame (600~1,200 s after the initiation), which was used for steady-state analysis with the continuous-infusion method, was visibly distinct compared with all of the frames obtained with the injection method. However, with the continuous-inhalation method, neither ventricle could be depicted because of high radioactivity in the lung on the right and lower-side images.

The radioactivity in the blood pool obtained by  $^{15}\text{O}$ -CO PET (Fig. 3g) and the gaseous volume estimated by inverse transmission data (Fig. 3h) were subtracted from the raw PET images (16th frame) with the continuous-inhalation and continuous-infusion methods, respectively (Fig. 3c and f). Both methods clearly delineated the myocardium after subtraction in comparison to the blood flow image (Fig. 3i). However, the continuous-inhalation method showed salient radioactivity on the lateral wall (Fig. 3c), whereas the continuous-infusion method showed only modest radioactivity in the myocardium (Fig. 3f). It is also notable that there was considerable radioactivity in the right ventricle with the continuous-infusion method even after the subtraction (Fig. 3f).

To further examine the differences between the continuous-infusion and continuous-inhalation methods, time-radioactivity curves during the PET scans were taken from four ROIs: the left ventricle (LV), right ventricle (RV), myocardium (Myo), and lung (Fig. 4). At the steady-state frame (600~1,200 s), the continuous-infusion method showed higher radioactivity in the RV and LV than in the myocardium (Fig. 4a), whereas the radioactivity of these regions was similar with the continuous-inhalation method (Fig. 4b). The radioactivity in LV was about two-thirds of that in RV in Fig. 4a, indicating that measurable radioactivity was excreted through the lung even after the femoral administration of  $^{15}\text{O}$ -O<sub>2</sub>. The lung excretion was also observed on the blood-subtracted image (Fig. 3e). Actually, there was significant radioactivity in the lung (Fig. 4a), although that was the lowest among the four ROIs. In contrast, the radioactivity in the myocardium was the lowest among the four ROIs with the continuous-inhalation method

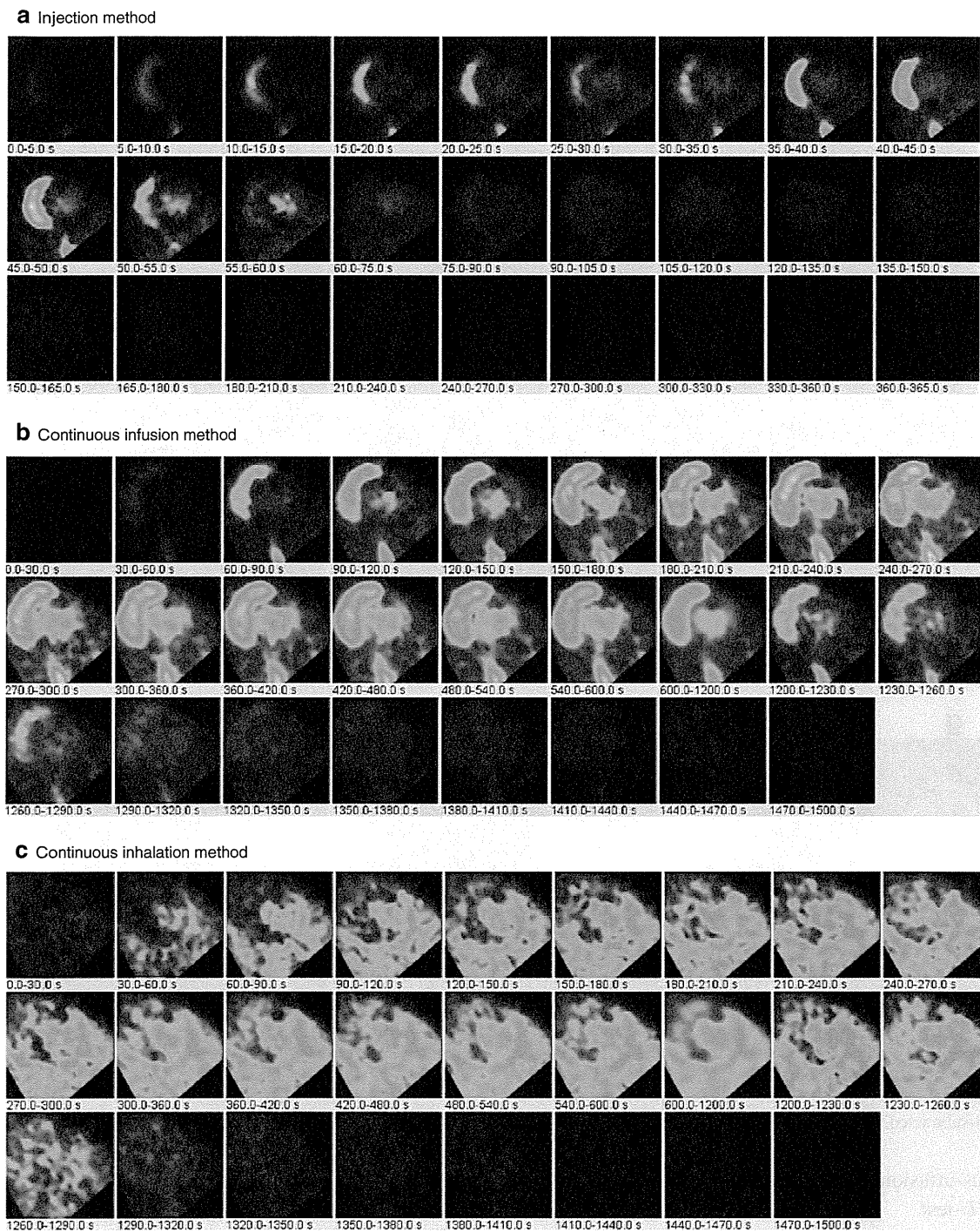


**Fig. 2** PET images obtained in (a) the injection method, (b) the continuous-infusion method with injectable  $^{15}\text{O-O}_2$ , and (c) the continuous-inhalation method with  $^{15}\text{O-O}_2$  gas

(Fig. 4b). The heart-to-lung radioactivity ratios were calculated from Fig. 4 for the quantitative estimation of image quality; the continuous-infusion method provided a ratio of  $1.38 \pm 0.24$ , whereas the ratio was less than one with the continuous-inhalation method.

Table 2 shows the quantitative OEF values in the lateral wall obtained by the injection, continuous-infusion, and

continuous-inhalation methods. These OEF values were consistent among the three methods.

Figure 5 represents the noise equivalent counts (NEC) standardized by the total counts detected by the PET scanner. Although the injection method tended to show rather high values, there was no significant difference between the values obtained by the injection and

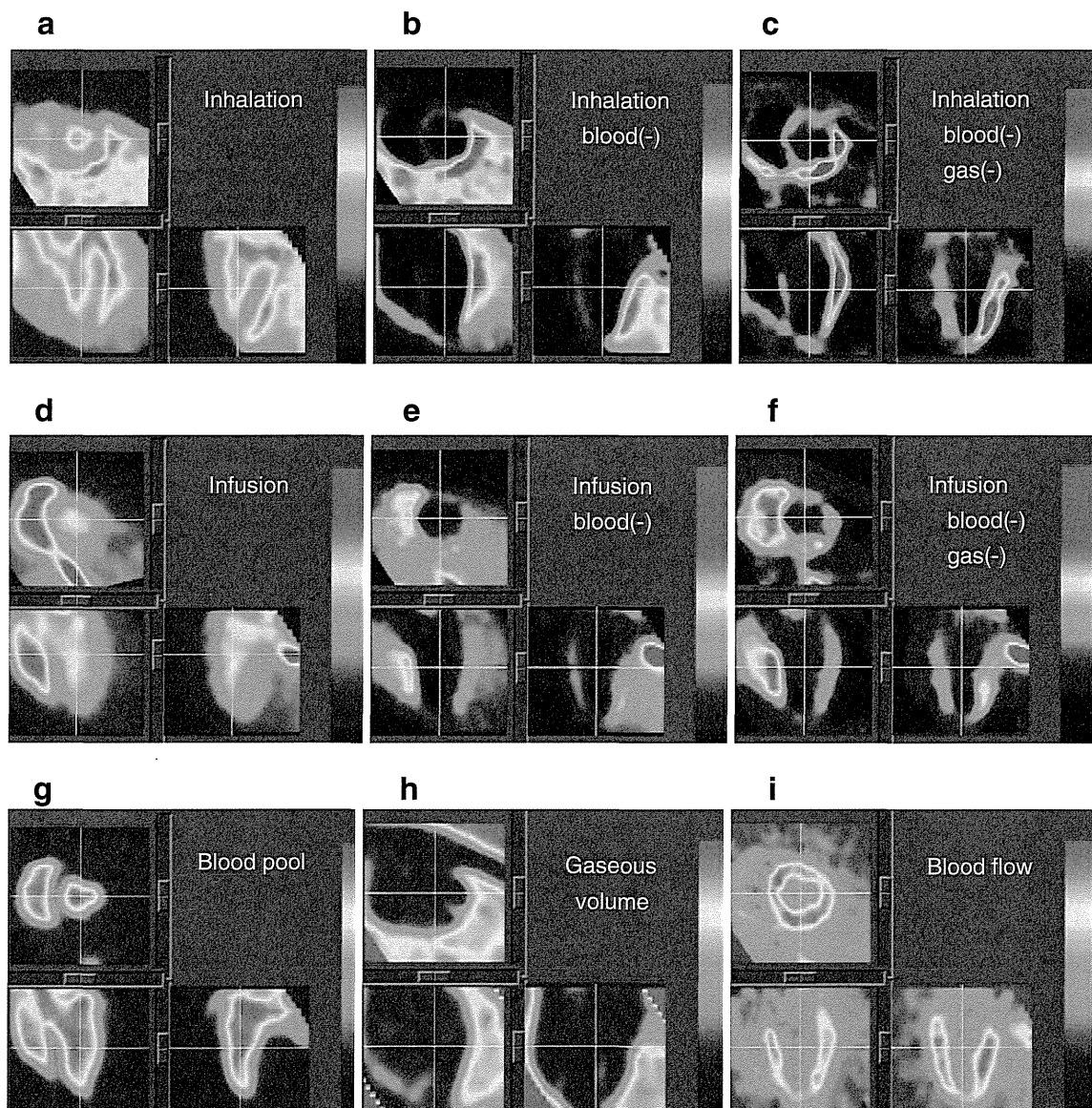


**Fig. 3** PET images obtained in the study are shown. The 16th frame (steady-state frames) of the continuous-inhalation method and the continuous-infusion method are shown in (a) and (d), respectively. The ‘blood-subtracted’ images shown in (b) and (e) were created by

subtraction of the blood-pool image by  $^{15}\text{O}$ -CO (g) from (a) and (d). The ‘blood- and gas-subtracted’ images shown in (c) and (f) were created by the successive subtraction of the gaseous image (h) from (b) and (e). The myocardial blood flow image is also shown in (i)

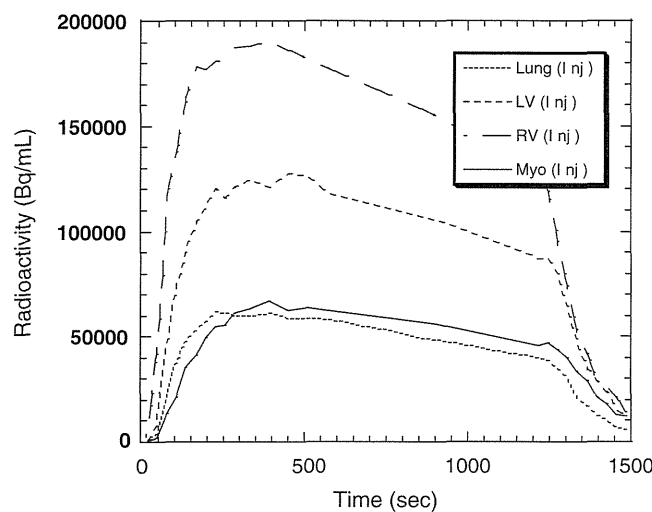
continuous-infusion methods as determined by a Mann Whitney *U*-test.

## Discussion

In previous studies, we showed the usefulness of the injectable  $^{15}\text{O}$ -O<sub>2</sub> system for estimating cerebral oxygen metabolism in small animals such as rats under normal or ischemic conditions [10–12]. Injectable  $^{15}\text{O}$ -O<sub>2</sub> replaced the inhalation protocol and radioactive  $^{15}\text{O}$ -O<sub>2</sub> was administered via the tail vein. Thus, injectable  $^{15}\text{O}$ -O<sub>2</sub> could abolish the artifact from the high radioactivity in the

inhalation tube that distorts the PET images, especially in small animals. We considered that the concept could also be utilized in the hearts of large animals. Therefore, in the present study, we tested the feasibility of an injectable  $^{15}\text{O}$ -O<sub>2</sub> system for estimating myocardial oxygen metabolism in normal pigs. In addition, since a shunt between the femoral artery and vein can be created in pigs but not in small animals, continuous infusion via the femoral shunt was also performed to achieve a constant and reliable delivery of radioactivity to the heart.

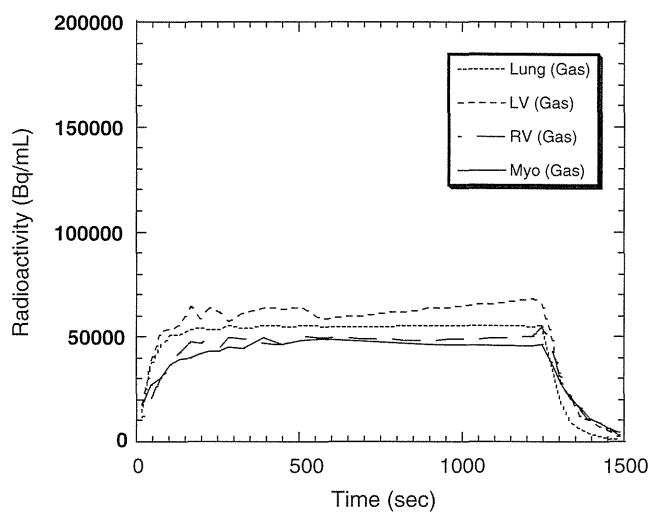
Dynamic PET scans showed a large difference in the radioactivity distribution among the three methods. Since the labeling efficiency to prepare injectable  $^{15}\text{O}$ -O<sub>2</sub> was

**a** Continuous infusion**Fig. 4** Time-activity curves from the left ventricle (LV), the right ventricle (RV), the myocardium (lateral wall, Myo) and a lung region with the continuous-infusion method (a) and the continuous-inhalation

lower with pig blood (ca. 61 MBq/ml at most) than with the blood of rats and humans (130 MBq/ml), the injection method provided rather obscure images. With the injection and continuous-infusion methods, the radioactivity in the lung was dramatically reduced in comparison to the continuous-inhalation method, since the heart-to-lung ratio with the continuous-infusion method was about 40% higher than with the continuous-inhalation method. This finding suggested that the two methods that inject radioactivity via a vein are more useful for analyzing myocardial oxygen metabolism in pigs than the continuous-inhalation method. However, a distinct difference between radioactivity of the right and left ventricles was observed in the images and time-radioactivity curves after venous administration of  $^{15}\text{O}$ -O<sub>2</sub>, indicating a certain degree of excretion of the radioactivity by the lung. Therefore, the spillover from the pulmonary alveoli to the myocardium could not be omitted in the two methods with venous administration, and Eq. (4)

**Table 2** OEF estimated by the three methods using injectable  $^{15}\text{O}$ -O<sub>2</sub> or  $^{15}\text{O}$ -O<sub>2</sub> gas

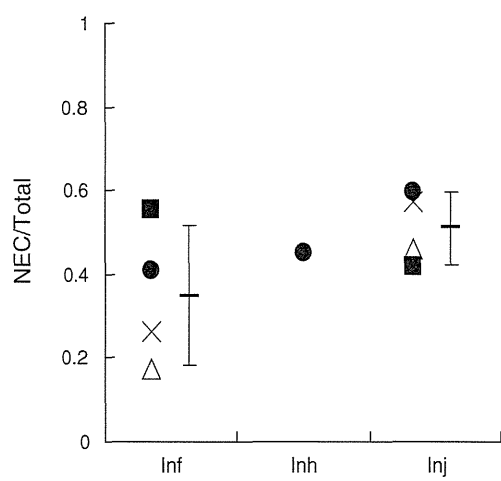
	OEF		
	Injection	Infusion	Inhalation
Pig. 1	0.70	0.72	
Pig. 2	0.67	0.72	
Pig. 3	0.71	0.74	
Pig. 4	0.76	0.69	0.72
Average	0.71	0.72	0.72
SD	0.036	0.020	

**b** Continuous inhalation

method (b). The supply of radioactivity was started at time 0 s and stopped at 1,200 s. The 16th frame for the steady-state analysis was 600–1,200 s

was used for the OEF analysis, although the radioactivity in the lung was lower than that in the myocardium.

On the other hand, with the continuous-inhalation method, the radioactivity of the lung was in between the radioactivity in the RV and LV. This is curious because  $^{15}\text{O}$  radioactivity was supplied from the inhalation tube and transferred from the lung to blood so that the radioactivity in the lung should have been the highest among the four ROIs. This may have been caused, in part, by inhomogeneous distribution of the radioactivity in the lung due to its structure in comparison with the myocardium and ventricles, and/or by artifacts from the lung to other

**Fig. 5** The ratio of noise equivalent counts (NEC) to total counts in the total field of view of the PET scanner obtained with the continuous-infusion method (Inf), the continuous-inhalation method (Inh) and the injection method (Inj)

tissues. In any case, it is notable that the radioactivity in the myocardium was the lowest with the continuous-inhalation method, leading to difficulty in analyzing myocardial oxygen metabolism.

The OEF values in lateral walls were calculated to compare the ability of the three methods to determine myocardial oxygen metabolism by using the blood flow derived from the dual-administration protocol with the injection method and the single-administration protocol with the two continuous methods. There was no difference in the blood flow between the two protocols. Consequently, the three methods provided the same OEF value of about 0.7 and this is a physiological value in normal pigs, as was previously demonstrated [17, 18]. We have demonstrated the potential of the injectable  $^{15}\text{O}$ -O<sub>2</sub> system for the estimation of physiological cerebral oxygen metabolism in rats and monkeys during early and late ischemia, hypertension, and ischemia plus hypertension [10–12, 19]. Therefore, we believe that the injection and continuous-infusion methods provide a physiological OEF in the myocardium. Nevertheless, we recognize the necessity to evaluate the reliability and usefulness of the injectable  $^{15}\text{O}$ -O<sub>2</sub> method in myocardial applications. Further studies using pathophysiological animal models are required in the future, such as myocardial ischemia, hypoxia, and heart failure. On the other hand, since MMRO<sub>2</sub> is basically regarded as the product of MBF and OEF, the results indicated that these three methods were equivalent in their ability to quantify MMRO<sub>2</sub> in normal pigs, at least in the lateral wall. Although the images after the subtraction of spillovers from blood and gas showed different contrast between the continuous-infusion and continuous-inhalation methods, the ability of these two methods to measure OEF and MMRO<sub>2</sub> in the lateral walls was equivalent.

We did not evaluate myocardial oxygen metabolism in other heart regions since the radioactivity in the right ventricle could not be removed due to a significant difference of radioactivity between the ventricles with the continuous-infusion method. The injection method might be able to evaluate oxygen metabolism in other regions besides the lateral wall, although this was not evaluated in this study due to the low radioactivity of injectable  $^{15}\text{O}$ -O<sub>2</sub> as described above. In the injection method, O-15 radioactivity was delivered from the femoral vein to RV, the lung, LV, and finally the myocardium. Thus, when the LV and myocardial activity reach a maximum, the RV activity is expected to be low. The later frames of the dynamic PET images with the injection method might avoid the high RV activity and delineate the myocardium and LV more clearly. With accurate anatomical information by gated PET/CT, the injection method will provide oxygen metabolism in other heart regions. In addition, the injection method has a benefit in that it is noninvasive and shortens the acquisition time in

comparison with the continuous-infusion method. Future studies are needed to determine whether the injectable  $^{15}\text{O}$ -O<sub>2</sub> system can be used in other heart regions.

With the injection method, the ratio of noise equivalent counts (NEC) to total counts tended to be the higher, probably because of the absence of high radioactivity adjacent to the PET scanner. Nevertheless, the continuous-infusion method did not show this tendency. This may be because tubes for the input to the artificial lung were positioned at the femoral shunt and the output to the drain of O-15 gas was positioned alongside the PET scanner, resulting in an increase of random counts during the study. Also, it is notable that the value with the continuous-inhalation method was not small, which suggests that the inhalation protocol itself did not worsen the results, but rather the high radioactivity in the lung might affect the analysis. In any case, if more care is given to shielding of the radioactivity in tubes and/or for arrangement of instruments in the PET room, a higher value of NEC/total counts will be obtained with the injectable  $^{15}\text{O}$ -O<sub>2</sub> system.

The declining slope delineated in the time-activity curves with the continuous-infusion method requires some explanation. Since the flow rate of O-15 gas supply to the artificial lung positioned at the femoral shunt was maintained constant during the PET scan, it is possible that a decrease of labeling efficiency of the artificial lung occurred due to the deposition of any components of blood. The blood of rats or humans was negligibly deposited in the artificial lung during circulation at the same rate for at least 30 min in our other experiments, so that this problem may be specific for pigs. It is unclear which component in pig blood was exactly involved in the deposition and three of four pigs did not show a declining slope of the time-activity curve.

In practice, in routine studies on myocardial oxygen metabolism using large animals such as pigs, the continuous-inhalation method with  $^{15}\text{O}$ -O<sub>2</sub> gas may be easier to perform for the following reasons: (1) the intubation tube used for gas anesthesia prior to the PET scan can also be used for  $^{15}\text{O}$ -O<sub>2</sub> gas inhalation; (2) catheterization of the femoral artery and vein to create the femoral shunt for the continuous-infusion method may be troublesome; and (3) the injection of  $^{15}\text{O}$ -O<sub>2</sub> requires an artificial lung, preparation time, and blood taken from the same animal prior to the PET scan. However, the injection of  $^{15}\text{O}$ -O<sub>2</sub> has a substantial advantage over the continuous-inhalation method in that there is reduced radioactivity in the lung and clearer images of the heart are obtained. Therefore, the method for estimating myocardial oxygen metabolism should be selected depending on the objectives of the study and the surgical procedures. Furthermore, since radioactivity administered into the femoral vein is partially excreted into expired air, the injectable  $^{15}\text{O}$ -O<sub>2</sub> system might be used for evaluating pulmonary function in the future.

## Conclusion

In this study, we tested the feasibility of using an injectable  $^{15}\text{O}$ - $\text{O}_2$  system to estimate myocardial oxygen metabolism in pigs. Both the bolus-injection and continuous-infusion methods reduced the radioactivity in the lung and provided similar OEF values in the lateral walls of the heart. These findings indicate that the injectable  $^{15}\text{O}$ - $\text{O}_2$  system has the potential to evaluate myocardial oxygen metabolism.

## References

- Ohtake T. The review of myocardial positron emission computed tomography and positron imaging by gamma camera. *Kaku Igaku*. 1998;35:179–87.
- Klein LJ, Visser FC, Knaapen P, Peters JH, Teule GJ, Visser CA, et al. Carbon-11 acetate as a tracer of myocardial oxygen consumption. *Eur J Nucl Med*. 2001;28:651–68.
- Schelbert HR. PET contributions to understanding normal and abnormal cardiac perfusion and metabolism. *Ann Biomed Eng*. 2000;28:922–9.
- Visser FC. Imaging of cardiac metabolism using radiolabelled glucose, fatty acids and acetate. *Coron Artery Dis*. 2001;12(Suppl 1):S12–8.
- Hata T, Nohara R, Fujita M, Hosokawa R, Lee L, Kudo T, et al. Noninvasive assessment of myocardial viability by positron emission tomography with  $^{11}\text{C}$  acetate in patients with old myocardial infarction. Usefulness of low-dose dobutamine infusion. *Circulation*. 1996;94:1834–41.
- Yamamoto Y, de Silva R, Rhodes CG, Iida H, Lammertsma AA, Jones T, et al. Noninvasive quantification of regional myocardial metabolic rate of oxygen by  $^{15}\text{O}_2$  inhalation and positron emission tomography. Experimental validation. *Circulation*. 1996;94:808–16.
- Iida H, Rhodes CG, Araujo LI, Yamamoto Y, de Silva R, Maseri A, et al. Noninvasive quantification of regional myocardial metabolic rate for oxygen by use of  $^{15}\text{O}_2$  inhalation and positron emission tomography. Theory, error analysis, and application in humans. *Circulation*. 1996;94:792–807.
- Shidahara M, Watabe H, Kim KM, Oka H, Sago M, Hayashi T, et al. Evaluation of a commercial PET tomograph-based system for the quantitative assessment of rCBF, rOEF and rCMRO<sub>2</sub> by using sequential administration of  $^{15}\text{O}$ -labeled compounds. *Ann Nucl Med*. 2002;16:317–27.
- Mintun MA, Raichle ME, Martin WR, Herscovitch P. Brain oxygen utilization measured with O-15 radiotracers and positron emission tomography. *J Nucl Med*. 1984;25:177–87.
- Magata Y, Temma T, Iida H, Ogawa M, Mukai T, Iida Y, et al. Development of injectable O-15 oxygen and estimation of rat OEF. *J Cereb Blood Flow Metab*. 2003;23:671–6.
- Temma T, Magata Y, Kuge Y, Shimonaka S, Sano K, Katada Y, et al. Estimation of oxygen metabolism in a rat model of permanent ischemia using positron emission tomography with injectable  $^{15}\text{O}$ - $\text{O}_2$ . *J Cereb Blood Flow Metab*. 2006;26:1577–83.
- Temma T, Kuge Y, Sano K, Kamihashi J, Obokata N, Kawashima H, et al. PET O-15 cerebral blood flow and metabolism after acute stroke in spontaneously hypertensive rats. *Brain Res*. 2008;1212:18–24.
- Watabe H, Jino H, Kawachi N, Teramoto N, Hayashi T, Ohta Y, et al. Parametric imaging of myocardial blood flow with  $^{15}\text{O}$ -water and PET using the basis function method. *J Nucl Med*. 2005;46:1219–24.
- Iida H, Rhodes CG, de Silva R, Yamamoto Y, Araujo LI, Maseri A, et al. Myocardial tissue fraction-correction for partial volume effects and measure of tissue viability. *J Nucl Med*. 1991;32:2169–75.
- Wienhard K, Dahlbom M, Eriksson L, Michel C, Bruckbauer T, Pietrzik U, et al. The ECAT EXACT HR: performance of a new high resolution positron scanner. *J Comput Assist Tomogr*. 1994;18:110–8.
- Kudomi N, Hayashi T, Teramoto N, Watabe H, Kawachi N, Ohta Y, et al. Rapid quantitative measurement of CMRO<sub>2</sub> and CBF by dual administration of  $^{15}\text{O}$ -labeled oxygen and water during a single PET scan-a validation study and error analysis in anesthetized monkeys. *J Cereb Blood Flow Metab*. 2005;25:1209–24.
- Alders DJ, Groeneveld AB, de Kanter FJ, van Beek JH. Myocardial  $\text{O}_2$  consumption in porcine left ventricle is heterogeneously distributed in parallel to heterogeneous  $\text{O}_2$  delivery. *Am J Physiol Heart Circ Physiol*. 2004;287:H1353–61.
- Van Woerkens EC, Trouwborst A, Duncker DJ, Koning MM, Boomstra F, Verdouw PD. Catecholamines and regional hemodynamics during isovolemic hemodilution in anesthetized pigs. *J Appl Physiol*. 1992;72:760–9.
- Temma T, Magata Y, Iida H, Hayashi T, Ogawa M, Mukai T, et al. Development of injectable O-15 oxygen and its application for estimation of OEF. International Congress Series, Quantitation in Biomedical Imaging with PET and MRI Proceedings of the International Workshop on Quantitation in Biomedical Imaging with PET and MRI. 2004;1265:262–65.

# Measurement of density and affinity for dopamine D<sub>2</sub> receptors by a single positron emission tomography scan with multiple injections of [<sup>11</sup>C]raclopride

Yoko Ikoma<sup>1,2</sup>, Hiroshi Watabe<sup>1</sup>, Takuya Hayashi<sup>1</sup>, Yoshinori Miyake<sup>1</sup>, Noboru Teramoto<sup>1</sup>, Kotaro Minato<sup>2</sup> and Hidehiro Iida<sup>1</sup>

<sup>1</sup>Department of Investigative Radiology, National Cardiovascular Center Research Institute, Osaka, Japan;

<sup>2</sup>Biomedical Imaging and Informatics, Graduate School of Information Science, Nara Institute of Science and Technology, Nara, Japan

Positron emission tomography (PET) with [<sup>11</sup>C]raclopride has been used to investigate the density ( $B_{max}$ ) and affinity ( $K_d$ ) of dopamine D<sub>2</sub> receptors related to several neurological and psychiatric disorders. However, in assessing the  $B_{max}$  and  $K_d$ , multiple PET scans are necessary under variable specific activities of administered [<sup>11</sup>C]raclopride, resulting in a long study period and unexpected physiological variations. In this paper, we have developed a method of multiple-injection graphical analysis (MI-GA) that provides the  $B_{max}$  and  $K_d$  values from a single PET scan with three sequential injections of [<sup>11</sup>C]raclopride, and we validated the proposed method by performing numerous simulations and PET studies on monkeys. In the simulations, the three-injection protocol was designed according to prior knowledge of the receptor kinetics, and the errors of  $B_{max}$  and  $K_d$  estimated by MI-GA were analyzed. Simulations showed that our method could support the calculation of  $B_{max}$  and  $K_d$ , despite a slight overestimation compared with the true magnitudes. In monkey studies, we could calculate the  $B_{max}$  and  $K_d$  of diseased or normal striatum in a 150 mins scan with the three-injection protocol of [<sup>11</sup>C]raclopride. Estimated  $B_{max}$  and  $K_d$  values of D<sub>2</sub> receptors in normal or partially dopamine-depleted striatum were comparable to the previously reported values.

*Journal of Cerebral Blood Flow & Metabolism* (2010) **30**, 663–673; doi:10.1038/jcbfm.2009.239; published online 11 November 2009

**Keywords:** [<sup>11</sup>C]raclopride; dopamine D<sub>2</sub> receptors; graphical analysis; multiple injections; positron emission tomography

## Introduction

Positron emission tomography (PET) with [<sup>11</sup>C]raclopride has been widely used to investigate the availability of striatal dopamine D<sub>2</sub> receptors *in vivo* (Farde *et al*, 1985; Köhler *et al*, 1985; Hall *et al*, 1988). A number of postmortem studies have shown that the abundance of dopamine D<sub>2</sub> receptor is elevated in striatum samples from untreated patients with Parkinson's disease (Guttman and Seeman, 1985; Seeman *et al*, 1987) and in schizophrenic patients who had never taken antipsychotics (Cross

*et al*, 1981; Joyce *et al*, 1988). The PET measurements have made it possible to quantify *in vivo* the density and apparent affinity of receptors by systematically varying the specific activity (or mass) of an administered radioligand (see for example, Farde *et al*, 1986). A study of Parkinson's disease by Rinne *et al* (1995) with *in vivo* PET showed increased density and unchanged affinity of dopamine D<sub>2</sub> receptors in the putamen in comparison with healthy controls. In corresponding studies of schizophrenia, early findings with [<sup>11</sup>C]N-methylspiperone indicated elevated D<sub>2</sub> binding, which was not replicated in some subsequent studies with [<sup>11</sup>C]raclopride (Wong *et al*, 1986; Farde *et al*, 1987, 1990). Dysfunction of dopamine receptors has also been suggested in other neurodegenerative or psychiatric diseases (e.g., multiple-system atrophy, progressive supranuclear palsy, and attention-deficit hyperactivity disorders); however, there have been only a few studies that

Correspondence: Dr H Watabe, Department of Investigative Radiology, National Cardiovascular Center Research Institute, 5-7-1, Fujishirodai, Suita, Osaka 565-8565, Japan.

E-mail: watabe@ri.ncvc.go.jp

Received 11 September 2009; revised 13 October 2009; accepted 19 October 2009; published online 11 November 2009

examined receptor function directly related to density and affinity. This might be due to the inherent difficulty in measuring absolute receptor abundance based on PET recordings.

In PET scans, to determine the density and affinity of receptors directly as parameters of kinetic model, it is necessary to apply a compartmental analysis based on a two-tissue compartment five-parameter model including density of receptors  $B_{\max}$  (pmol/mL), bimolecular association rate constant  $k_{on}$  (mL/pmol/min), and unimolecular dissociation rate constant  $k_{off}$  (min<sup>-1</sup>) (Farde *et al*, 1989). However, since data from a single PET scan are not enough to determine the  $B_{\max}$  and  $k_{on}$  individually, multiple PET scans should be taken with different molar amounts of injected ligand. In addition, model parameters are estimated by a nonlinear least squares fitting with the metabolite-corrected plasma input function, so the solutions are often unstable and sensitive to statistical noise, and invasive arterial sampling is required to use this method.

Farde *et al* (1986, 1989) determined the value of  $B_{\max}$  and apparent affinity  $K_d$  ( $=k_{off}/k_{on}$ ) by a graphical analysis using a time-activity curve (TAC) of the specifically bound target region and a reference region where specific bindings are negligible. In this method, the ratio of specific bound and free ligand concentrations at the equilibrium state are plotted versus the concentration of specific bound ligand, and  $B_{\max}$  and  $K_d$  are estimated from the slope and intercept of the regression line. Other groups also used the value of distribution volume ratio – 1 estimated from the graphical analysis of Logan *et al* (1996), instead of the ratios of specific bound and free concentration, to obtain stable values of the y-axis quantity (Logan *et al*, 1997; Doudet and Holden, 2003; Doudet *et al*, 2003). These methods are practical, because they do not require arterial blood sampling, and their respective estimation processes are easy to carry out. However, to estimate the regression line of a graphical plot, multiple PET scans (at least two or three) are required under variable molar amounts of administered ligand, so scans have been performed on separate days. Even in quantitative PET scans, the separate day protocol may suffer from interday or intraday variations in physiologic conditions, such as cerebral blood pressure, flow, and receptor bindings, which may affect the accuracy of the estimates.

We developed a method, called the multiple-injection simplified reference tissue model (MI-SRTM), to measure the change in binding potential ( $BP_{ND} = k_3/k_4$  (Mintun *et al*, 1984)) of dopamine D<sub>2</sub> receptors from a single session of PET scanning with multiple injections of [<sup>11</sup>C]raclopride (Watabe *et al*, 2006; Ikoma *et al*, 2009), and we showed that this method could detect the change in  $BP_{ND}$  because of an increase in mass of administered [<sup>11</sup>C]raclopride in a short scanning period, which is a prerequisite for measuring the saturation binding parameters as steady state. In this study, we extend our earlier

report for estimating  $B_{\max}$  and  $K_d$  from a single session of PET scanning with triple injections of [<sup>11</sup>C]raclopride using MI-SRTM and the graphical analysis, and we validated the proposed method by performing numerous simulations and studies on monkeys using PET and [<sup>11</sup>C]raclopride.

## Materials and methods

### Theory

**Graphical Analysis with a Reference Region for Estimation of Density and Affinity:** Graphical analysis based on the Scatchard plot (Scatchard, 1949) has been used to estimate the values of  $B_{\max}$  and  $K_d$  from a series of PET recordings with various molar amounts of administered ligand (Farde *et al*, 1986). In brief, the ratios ( $B/F$ ) of specific bound ligand concentration ( $B$  [pmol/mL]) and free ligand concentration ( $F$  [pmol/mL]) at equilibrium are plotted versus  $B$ . In this plot, the slope and x-intercept represent  $-1/K_d$  and  $B_{\max}$ , respectively. In general, for graphical analysis without arterial blood sampling, the total radioligand concentration in the reference region ( $C_r$  [Bq/mL]), where specific bindings are negligible, is used as an estimate of the free radioligand concentration in the target region ( $C_t$  [Bq/mL]), that is  $C_t^{\text{ref}} = C_r$ , and the specific binding radioligand concentration in the target region ( $C_b$  [Bq/mL]) is defined as radioactivity in the target region ( $C_t$  [Bq/mL]) reduced with  $C_r$ , that is  $C_b^{\text{ref}} = C_t - C_r$  (Figure 1). The radioactivity concentrations of  $C_t^{\text{ref}}$  and  $C_b^{\text{ref}}$ , at the point in time when  $dC_b^{\text{ref}}/dt = 0$  ( $T_{eq}$ ), are divided by a specific activity of the administered ligand, and used as  $F$  and  $B$  at the transient equilibrium in the graphical analysis

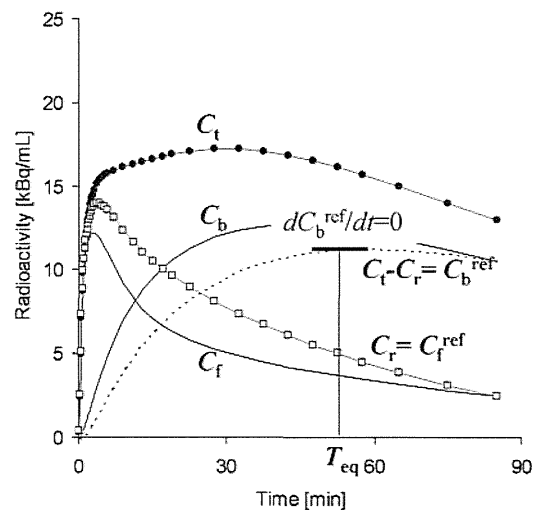


**Figure 1** An example of simulated TACs for the striatum ( $C_t$ ), free ( $C_f$ ), and specific bound ( $C_b$ ) concentrations in the striatum, the cerebellum used as a reference region ( $C_r$ ) and bound concentration in the striatum estimated using a reference region ( $C_b^{\text{ref}} = C_t - C_r$ ) with  $K_1 = 0.033$ ,  $K_1/K_2 = 0.59$ ,  $k_{on} = 0.0033$ ,  $B_{\max} = 25.7$ ,  $k_4 = 0.034$  for the striatum, and  $K_1 = 0.034$ ,  $K_1/K_2 = 0.36$ ,  $k_3 = 0.022$ ,  $k_4 = 0.034$  for the cerebellum. The time point of  $dC_b^{\text{ref}}/dt = 0$  ( $T_{eq}$ ) is considered the transient equilibrium, and bound concentration at the equilibrium ( $B^{\text{ref}}$ ) is obtained from the radioactivity concentration of  $C_b^{\text{ref}}$  at  $T_{eq}$ .

(Farde *et al*, 1989). In our study, we use the nomenclature  $B^{\text{ref}}$  and  $F^{\text{ref}}$  to represent the concentrations otherwise known as  $B$  and  $F$ . The value of the  $y$  axis,  $B^{\text{ref}}/F^{\text{ref}}$ , is sometimes replaced by the binding potential estimated by the graphical analysis of Logan *et al* (1996) or some other method (Logan *et al*, 1997; Doudet and Holden, 2003; Doudet *et al*, 2003).

**Multiple-Injection Simplified Reference Tissue Model for Estimation of Binding Potential:** A simplified reference tissue model (SRTM) can provide three parameters ( $R_i$ ,  $k_2$ ,  $\text{BP}_{\text{ND}}$ ) without invasive arterial blood sampling by using a TAC of the reference region (Lammertsma and Hume, 1996). The MI-SRTM extended this SRTM for sequential multiple injections in a single session of PET scanning by taking into account the residual radioactivity in the target tissue at the time of each injection. As such, the magnitude of  $\text{BP}_{\text{ND}}$  for the  $i$ th injection is described in the following terms (Ikoma *et al*, 2009):

$$C_{ti}(t) = R_{1i}C_{ri}(t) + \left( k_{2i} - \frac{R_{1i}k_{2i}}{1 + \text{BP}_{\text{ND}i}} \right) e^{-\frac{k_{2i}}{1 + \text{BP}_{\text{ND}i}}t} \otimes C_{ri}(t) + (C_{ti}(0) - R_{1i}C_{ri}(0)) e^{-\frac{k_{2i}}{1 + \text{BP}_{\text{ND}i}}t} \quad (1)$$

where  $C_{ti}$  and  $C_{ri}$  are the radioactivity concentrations in the target and reference region, respectively, and  $t$  is the time from the start of the  $i$ th injection.

**Multiple-Injection Graphical Analysis for Estimation of Density and Affinity:** The conventional graphical analysis was applied to the  $B_{\text{max}}$  and  $K_d$  estimations with the multiple-injection approach. In this multiple-injection graphical analysis (MI-GA), the  $\text{BP}_{\text{ND}}$  calculated for each injection using MI-SRTM was plotted as a function of the concentration of specific bound raclopride at the transient equilibrium ( $B^{\text{ref}}$  [pmol/mL]) within the scan duration for each injection, and  $B_{\text{max}}$  and  $K_d$  were estimated from the regression line.

In this study for  $[^{11}\text{C}]$ raclopride, the TAC of the cerebellum was used as the reference TAC. Each parameter in the MI-SRTM was estimated by nonlinear least squares fitting with iteration of the Gauss–Newton algorithm. It should be noted that the transient equilibrium condition is required for each injection in the MI-GA.

## Simulation Analysis

Simulations were performed to determine the range of administered mass of three injections and to evaluate feasibility of the MI-GA to estimate the  $B_{\text{max}}$  and  $K_d$ .

**Effect of Injected Mass on  $\text{BP}_{\text{ND}}$  Estimates:** To investigate the effect of the administered molar amount of  $[^{11}\text{C}]$ raclopride on  $\text{BP}_{\text{ND}}$  estimates and to determine the molar amount of three injections for monkey studies, a relationship between  $\text{BP}_{\text{ND}}$  and  $B^{\text{ref}}$  was obtained by a computer simulation. Noiseless TACs of the striatum and cerebellum were generated with a measured plasma TAC and assumed parameter values derived from measurements taken from the monkey studies. The TAC of the cerebellum was simulated with a conventional two-tissue compartment

four-parameter model with assumed parameter values obtained earlier in our monkey studies:  $K_1 = 0.034$  (mL/mL/min)  $K_1/k_2 = 0.36$ ,  $k_3 = 0.022$  ( $\text{min}^{-1}$ ),  $k_4 = 0.034$  ( $\text{min}^{-1}$ ). Meanwhile, the TAC of the striatum was simulated with a two-tissue compartment five-parameter model expressed as Equation (2) by solving these differential equations with the numerical analysis of fourth-order Runge–Kutta method with assumed parameter values  $K_1 = 0.033$  (mL/mL/min),  $K_1/k_2 = 0.59$ ,  $k_{\text{on}} = 0.0033$  (mL/ pmol/min),  $B_{\text{max}} = 25.7$  (pmol/mL),  $k_4 = 0.026$  ( $\text{min}^{-1}$ ), and  $\text{SA} = 37$  (GBq/ $\mu$ mol):

$$\begin{aligned} \frac{dC_f}{dt} &= K_1 C_p(t) - (k_2 + k_3(t)) C_f(t) + k_4 C_b(t) \\ \frac{dC_b}{dt} &= k_3(t) C_f(t) - k_4 C_b(t) \\ k_3(t) &= k_{\text{on}} \left( B_{\text{max}} - \frac{C_b(t)}{\text{SA}} \right) \end{aligned} \quad (2)$$

where  $C_f$  and  $C_b$  are the concentrations of radioactivity for free and specifically bound  $[^{11}\text{C}]$ raclopride in tissue, respectively; and  $\text{SA}$  is the specific activity of administered  $[^{11}\text{C}]$ raclopride.

As reference, the relationships between  $B^{\text{ref}}$  and  $\text{BP}_{\text{ND}}$  or  $B^{\text{ref}}/F^{\text{ref}}$  were investigated in the case of a single injection of  $[^{11}\text{C}]$ raclopride by varying injected mass. TACs of the striatum and cerebellum for the single injection with a 50 mins scan were generated using the measured plasma TAC of a single injection in which the input plasma TAC was amplified, such that the corresponding mass increased from 1 to 500 nmol per injection. In each simulated TAC,  $\text{BP}_{\text{ND}}$  values were estimated by the SRTM, and then,  $B^{\text{ref}}/F^{\text{ref}}$  and  $B^{\text{ref}}$  were calculated by the transient equilibrium with the cerebellum TAC.

Next, TACs of the striatum and cerebellum for three injections at 50 mins intervals were generated using the plasma TAC of three sequential injections in which the input plasma TAC was amplified so that the mass of the first and second injections would be 1.5 and 10 nmol/kg, and the mass of the third injection would be 1.5 to 150 nmol/kg. In each simulated TAC,  $\text{BP}_{\text{ND}}$  values were estimated by the MI-SRTM, and  $B^{\text{ref}}/F^{\text{ref}}$  and  $B^{\text{ref}}$  for the third injection was calculated by the transient equilibrium with the cerebellum TAC. The relationships between  $B^{\text{ref}}$  and  $\text{BP}_{\text{ND}}$  or  $B^{\text{ref}}/F^{\text{ref}}$  for the third injection were investigated, and compared with that for the single injection.

**Estimation of  $B_{\text{max}}$  and  $K_d$  Values by the Multiple-Injection Graphical Analysis:** The reliability of  $B_{\text{max}}$  and  $K_d$  estimates by the graphical analysis was investigated for the proposed sequential multiple-injection approach (single PET scan) and compared with that for the conventional nonsequential approach (three PET scans on different days, such that no residual mass remained). Noiseless TACs of the striatum and cerebellum were simulated using assumed parameters of the two-tissue compartment model mentioned above and the plasma input function for three injections in which the magnitude of each ‘virtual’ input function was adjusted so that the injection mass would be 1.5, 10, or 30 nmol/kg determined from the simulation study mentioned above, with 50 mins intervals as reported

by Ikoma *et al* (2009). In the striatum TACs,  $B_{\max}$  values were varied from 10 to 50 pmol/mL at 5 pmol/mL intervals with other parameters fixed ( $K_d = 7.9$  pmol/mL), or  $K_d$  was varied from 3 to 15 at 2 pmol/mL intervals by changing  $k_{on}$  with other parameters fixed ( $B_{\max} = 25.7$  pmol/mL). For each TAC,  $B_{\max}$  and  $K_d$  were estimated by the MI-GA from three points obtained by MI-SRTM for the single PET scan approach and they were estimated by the graphical analysis from three points obtained by the conventional SRTM for the three PET scan approach. Then, estimates were compared with the true values. In the single PET scan approach,  $B_{\max}$  and  $K_d$  were also estimated without reference TAC by the MI-GA from three points of  $BP_{ND}$  and  $B$  obtained by the two-tissue compartment four-parameter model with the plasma input function shown in the Appendix.

### Analysis of Monkey Studies

PET studies were performed on three cynomolgus macaques (weight  $6.9 \pm 2.1$  kg) with the multiple-injection approach. One animal (monN) was a healthy monkey aged 5 years, and the others had a syndrome acquired Parkinsonism. Of these, one (monUP, aged 7 years) had hemiparkinsonism induced by injecting the selective neurotoxin, *N*-methyl-4-phenyl-1,2,3,6-tetrahydropyridine (MPTP) (0.4 mg/kg) into the right carotid artery (Bankiewicz *et al*, 1986), whereas the other (monBP, aged 5 years) had bilateral Parkinsonism induced by injecting MPTP (0.4 mg/kg) intravenously and intermittently (twice a week for a total of 14 injections) (Takagi *et al*, 2005). Each Parkinsonian animal showed typical Parkinsonian symptoms in the limbs (motor slowness, tremor) unilaterally or bilaterally. The PET scan was performed after the symptom reaching stable (6 months after the first injection of MPTP). Anesthesia was induced with ketamine (8.4 mg/kg, intramuscularly) and xylazine (1.7 mg/kg, intramuscularly) and maintained by intravenous propofol (6 mg/kg/h) and vecuronium (0.02 mg/kg/h) during the scan. The monkeys were maintained and handled in accordance with guidelines for animal research on Human Care and Use of Laboratory Animals (Rockville, National Institutes of Health/Office for Protection from Research Risks, 1996). The study protocol was approved by the Subcommittee for Laboratory Animal Welfare of the National Cardiovascular Center.

After the synthesis of  $[^{11}\text{C}]$ raclopride, nonradioactive raclopride was added so that targeted molar amount of raclopride would be administered for three injections (1.5, 10, and 30 nmol/kg); this was done by dividing the  $[^{11}\text{C}]$ raclopride diluted by nonradioactive raclopride into three portions with different volumes, containing the intended masses of raclopride. For the first injection,  $1.9 \pm 0.16$  nmol/kg ( $57.0 \pm 5.7$  MBq) of  $[^{11}\text{C}]$ raclopride was administered by a bolus injection at the beginning of the scan. Fifty minutes later, the second  $[^{11}\text{C}]$ raclopride injection,  $11.1 \pm 0.56$  nmol/kg ( $60.4 \pm 8.8$  MBq at the time of second injection) was administered by a bolus, and 50 mins after that, a bolus of  $31.1 \pm 2.1$  nmol/kg ( $30.8 \pm 4.4$  MBq at the time of third injection) of  $[^{11}\text{C}]$ raclopride was administered

again. Data were acquired for 150 mins (10 secs  $\times$  18, 30 secs  $\times$  6, 120 secs  $\times$  7, 300 secs  $\times$  6; total 50 mins for each injection). The specific radioactivity was  $4.7 \pm 2.2$  GBq/ $\mu\text{mol}$  at the time of the first injection.

PET scans were performed using a PCA-2000A positron scanner (Toshiba Medical Systems Corporation, Otawara, Japan) that provides 47 planes and a 16.2 cm axial field-of-view. The transaxial and axial spatial resolution of the PET scanner were 6.3 and 4.7 mm full width at half maximum (Herzog *et al*, 2004). A transmission scan with a 3-rod source of  $^{68}\text{Ge}$ - $^{68}\text{Ga}$  was performed for 20 mins for attenuation correction before the administration of  $[^{11}\text{C}]$ raclopride. Radioactivity was measured in the three-dimensional mode and the data were reconstructed by a filtered back-projection using a Gaussian filter (3 mm of full width at half maximum). Region-of-interests (ROIs) were defined manually over the left and right striatum and cerebellum for PET images, and the radioactivity concentrations in these regions were obtained. For the left and right striatum,  $R_1$ ,  $k_2$ , and  $BP_{ND}$  for each injection were estimated by the MI-SRTM. In addition, parametric images were generated, estimating each parameter voxel by voxel, using the MI-SRTM with a basis function method in which the model Equation (1) was solved using linear least squares for a set of basis functions, which enables the incorporation of parameter bounds (Gunn *et al*, 1997; Ikoma *et al*, 2009).  $B_{\max}$  and  $K_d$  were estimated by the MI-GA from these  $BP_{ND}$  values of left and right striatum for three injections.

In the unilateral Parkinsonian animal, three PET scans with conventional single injection with different masses of  $[^{11}\text{C}]$ raclopride were also performed for comparison with results by the multiple-injection single PET scan approach. A PET scan with a bolus injection of 2.1 nmol/kg (50.6 MBq), 11.3 nmol/kg (60.4 MBq), or 31.1 nmol/kg (30.8 MBq) of  $[^{11}\text{C}]$ raclopride was obtained on separate days. PET data were acquired for 50 mins with the same protocol as the single PET scan approach. The values of  $R_1$ ,  $k_2$ , and  $BP_{ND}$  were estimated by the SRTM, and  $B_{\max}$  and  $K_d$  were estimated by the conventional graphical analysis.

## Results

### Simulation Study

**Effect of Injected Mass on  $BP_{ND}$  Estimates:** In the simulations, the value of  $BP_{ND}$ , estimated by the MI-SRTM, decreased as injected molar amount of raclopride increased, that is, concentration of bound raclopride became larger. The relationship between  $BP_{ND}$  and  $B^{\text{ref}}$  had a good linear correlation to some extent; however, it did not remain linear for large  $B^{\text{ref}}$  (Figure 2A). The regression line where  $B^{\text{ref}} < 20$  pmol/mL was  $BP_{ND} = -0.091B^{\text{ref}} + 2.4$ ,  $R^2 = 0.997$  for the first injection. In the relationship between  $BP_{ND}$  and  $B^{\text{ref}}$ ,  $BP_{ND}$  values of the third injection were higher than those of the first injection when  $B^{\text{ref}}$  was lower than 20 pmol/mL. The ratio  $B^{\text{ref}}/F^{\text{ref}}$  was almost the same as the  $BP_{ND}$  estimated by MI-SRTM, though it was a little smaller when  $B^{\text{ref}}$  was lower than 5 pmol/mL (Figure 2B).

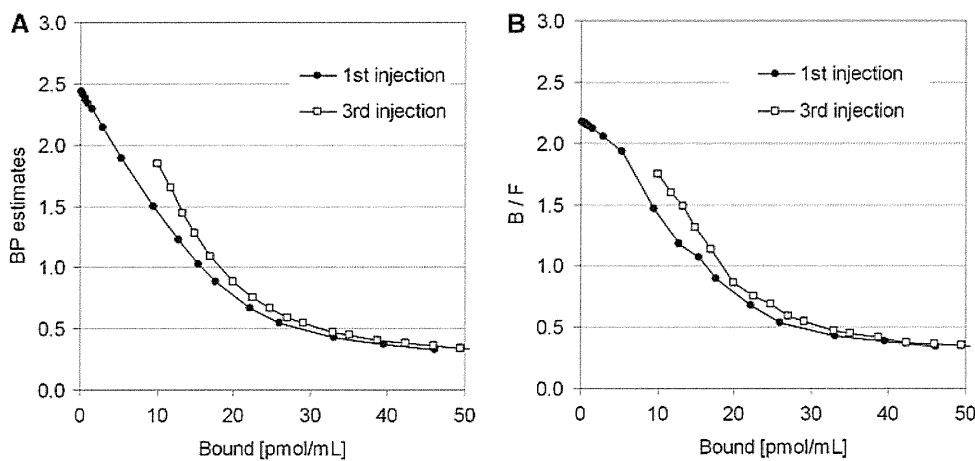


**Figure 2** Relationship between specifically bound concentration and  $BP_{ND}$  (A) or  $B^{\text{ref}}/F^{\text{ref}}$  (B) estimates for the first and third injection in the simulations.

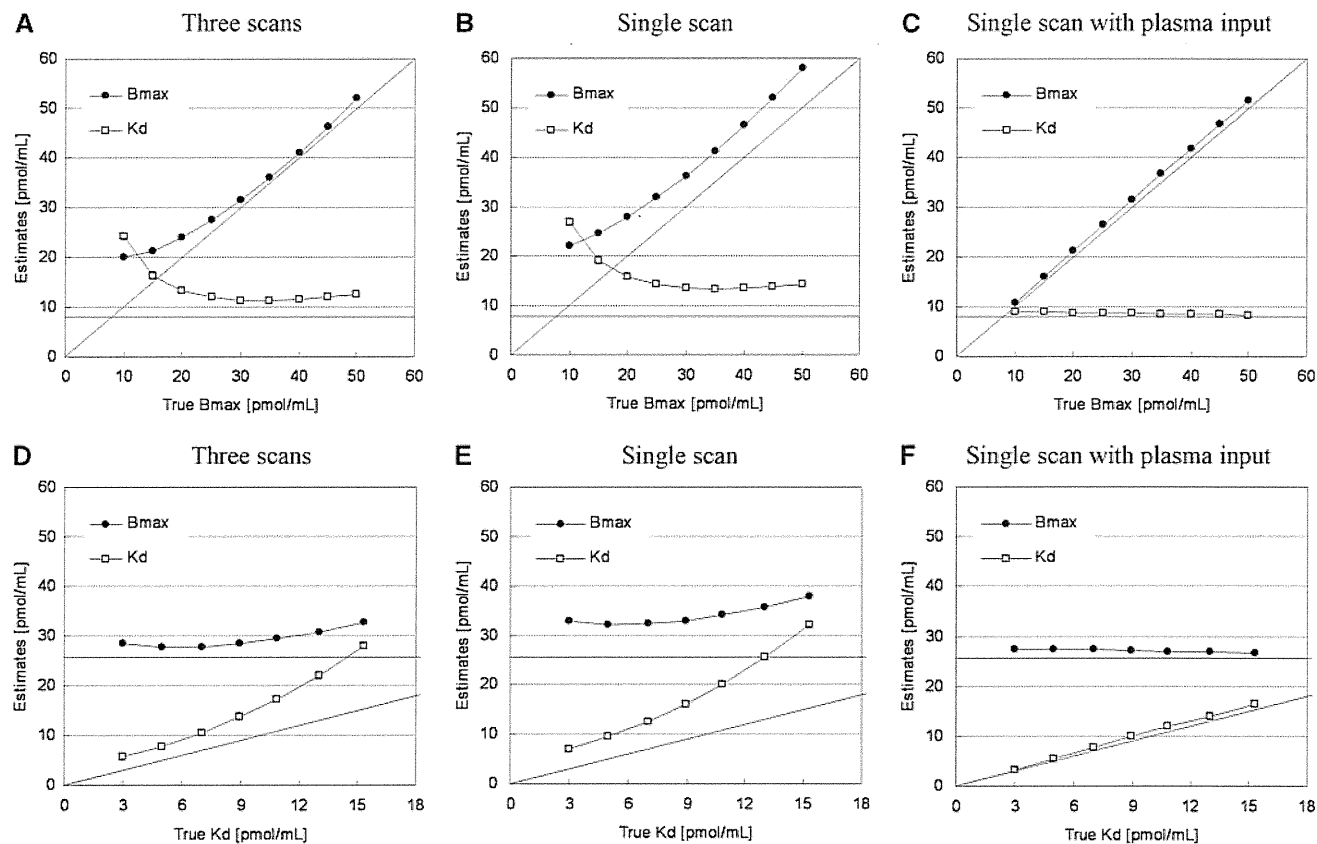


**Figure 3** Relationships between estimates and true values of  $B_{\text{max}}$  and  $K_d$  for simulated TACs with various  $B_{\text{max}}$  and fixed  $K_d$  (A-C) and with various  $K_d$  and fixed  $B_{\text{max}}$  (D-F) by the three PET scan approach (A, D), multiple-injection single PET scan approach (B, E), and single PET scan approach with the plasma input function (C, F).

**Estimation of  $B_{\text{max}}$  and  $K_d$  Values by the Multiple-Injection Graphical Analysis:** The TACs were calculated for a range of possible  $B_{\text{max}}$  and  $K_d$  values, and the relationship between true and estimated  $B_{\text{max}}$  or  $K_d$  values was investigated for conventional three PET scan and the proposed single PET scan approaches. When  $B_{\text{max}}$  was varied,  $B_{\text{max}}$  and  $K_d$  were overestimated compared with the true values in both three PET scan and single PET scan approaches

(Figures 3A and 3B). However, a good correlation was observed between true and estimated  $B_{\text{max}}$ , and there was little variation in estimated  $K_d$  when  $B_{\text{max}}$  was set higher than 20 pmol/mL. Similarly, when  $K_d$  was varied, although  $K_d$  and  $B_{\text{max}}$  were overestimated in both approaches, there was a good correlation between true and estimated  $K_d$ , and estimated  $B_{\text{max}}$  was constant (Figures 3D and 3E). In both cases,  $B_{\text{max}}$  and  $K_d$  estimates in the single

PET scan approach were higher than those in the three PET scan approach. In the TAC simulated with  $B_{max} = 25.7$  and  $K_d = 7.0$ , estimated  $B_{max}$  and  $K_d$  were 27.8 and 10.5, respectively, in the three PET scan approach, and 32.3 and 12.6, respectively, in the single PET scan approach. In contrast to these approaches with the reference TAC, the overestima-

tion of  $B_{max}$  and  $K_d$  was scarcely observed in the MI-GA with the plasma input function (Figures 3C and 3F).

### Monkey Studies

Typical examples of TACs for the striatum and the cerebellum in the multiple-injection study are shown in Figure 4, and the parametric images of  $BP_{ND}$  for the first, second, and third injection, and images of  $B_{max}$  and  $K_d$  for the voxels in which  $BP_{ND1}$  was higher than 1.5 are shown in Figure 5. The estimated  $BP_{ND}$  decreased as the injected molar amount of  $[^{11}C]$ raclopride became larger in the second or third injection. Estimated  $BP_{ND1}$ ,  $BP_{ND2}$ , and  $BP_{ND3}$  values were 2.3, 1.4, and 0.74, respectively, in the left striatum, and 2.6, 1.9, and 0.87, respectively, in the right striatum. The reduction in  $BP_{ND}$  was also observed in the parametric images.

The plots of MI-GA are shown in Figure 6. Plots of MI-GA for each of three animals were on the line, and  $B_{max}$  and  $K_d$  could be estimated as summarized in Table 1. Using the single scan approach for the hemiparkinsonian animal,  $B_{max}$  was 42.3 pmol/mL and  $K_d$  was 15.2 pmol/mL in the affected (right) striatum, and  $B_{max}$  was 32.3 pmol/mL and  $K_d$  was 13.0 pmol/mL in the contralateral (left) normal striatum. Corresponding estimates for the three scan approach were  $B_{max} = 36.4$  and  $K_d = 13.3$  pmol/mL in the right striatum and  $B_{max} = 29.2$  and  $K_d = 11.6$  pmol/mL in the

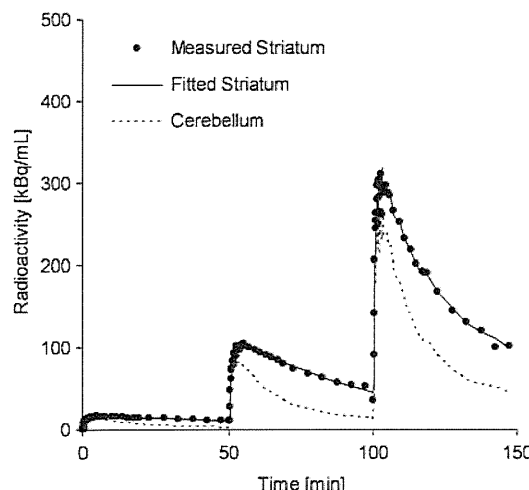


**Figure 4** Measured TACs of the striatum and cerebellum and a fitted curve for the striatum using MI-SRTM in the monkey study by a single scan with sequential three injections of  $[^{11}C]$ raclopride.

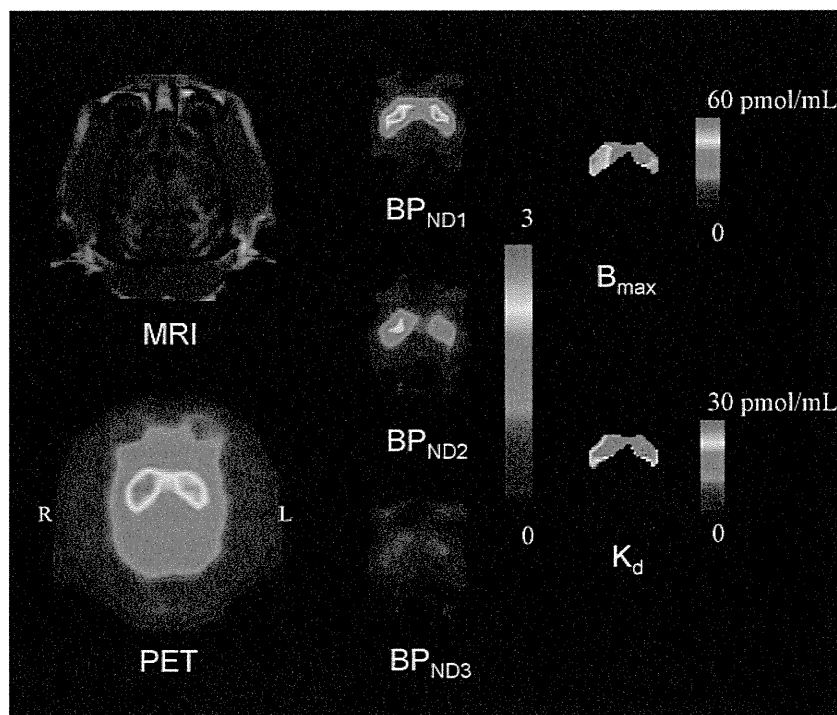


**Figure 5** MRI and PET summation image (left) and parametric images of  $BP_{ND}$  for the first, second, and third injection (center) and parametric images of  $B_{max}$  and  $K_d$  for the voxels in which  $BP_{ND1}$  is higher than 1.5 (right) in the unilateral Parkinsonian (monUP) monkey study by a single scan with three sequential injections of  $[^{11}C]$ raclopride. Although ROI analysis disclosed higher  $B_{max}$  values in the MPTP-infused side of the striatum, the parametric image showed more evident increase of  $B_{max}$  in the dorsal and posterior parts of the striatum.

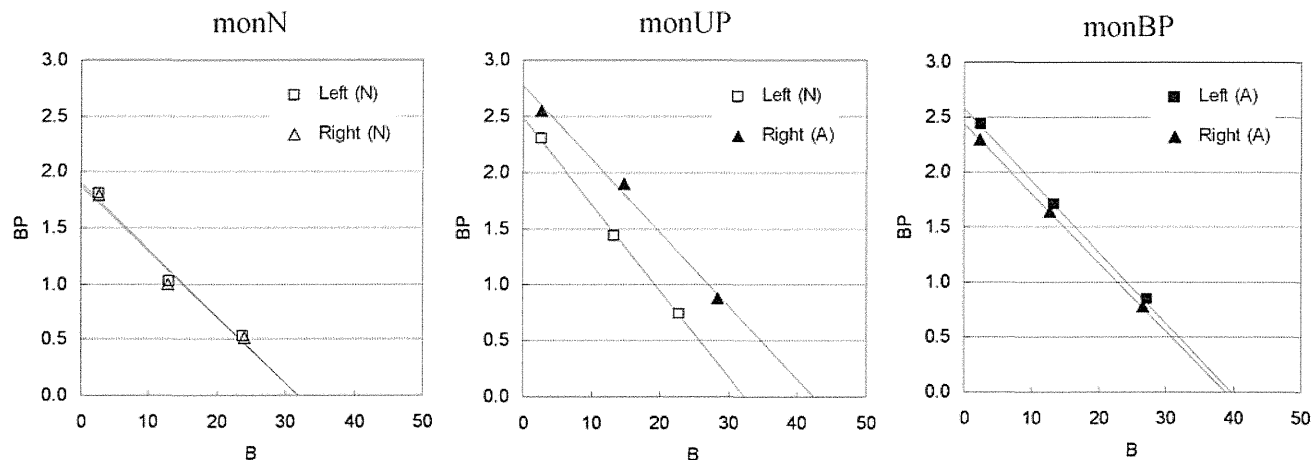


**Figure 6** Single-scan, multiple-injection graphical analysis for normal (N) or affected (A) region of the left or right striatum in three monkeys that were normal (monN), unilateral Parkinsonian (monUP), and bilateral Parkinsonian (monBP).

**Table 1** Estimated  $B_{\max}$  and  $K_d$  values in three monkey studies

Scan protocol	Subject	Region	Diagnosis	$B_{\max}$ (pmol/mL)	$K_d$ (pmol/mL)
Single scan	monN	L	N	31.8	16.7
		R	N	31.7	16.9
	monUP	L	N	32.3	13.0
		R	A	42.3	15.2
	monBP	L	A	39.6	15.4
		R	A	38.7	15.9
Three scans	monUP	L	N	29.2	11.6
		R	A	36.4	13.3

L, left striatum; R, right striatum; N, normal striatum; A, affected striatum.

left striatum. Both  $B_{\max}$  and  $K_d$  of the single PET scan approach were slightly higher than those of the three PET scan approach. However, importantly, both approaches found that  $B_{\max}$  in the affected striatum was higher than that in the normal striatum. The bilateral Parkinsonian animal showed  $B_{\max}$  values of left = 39.6 pmol/mL, right = 38.7 pmol/mL, both of which were higher than those of the striatum of the normal animal or the normal striatum of the unilateral animal, but were very close to the affected striatum of the unilateral animal. The  $K_d$  values of the bilateral animal were not so different from other striatums.

## Discussion

### Density and Affinity Determination by Graphical Analysis with the Reference Region

In the graphical analysis for PET receptor studies, the values of  $B_{\max}$  and  $K_d$  were estimated from the relationship between the ratio of bound to free concentrations and bound concentration at the time of transient equilibrium, using the TAC of the reference region (Farde *et al*, 1986). Some groups have used the value estimated from the distribution

volume ratio – 1, instead of the  $B^{\text{ref}}/F^{\text{ref}}$  value of the y axis, because the values of  $B^{\text{ref}}/F^{\text{ref}}$  could change considerably with small changes in the time point of the transient equilibrium  $T_{\text{eq}}$  determined as the maximum  $C_b^{\text{ref}}$  (Logan *et al*, 1997; Doudet and Holden, 2003; Doudet *et al*, 2003). Distribution volume ratio or  $BP_{\text{ND}}$  is estimated from the kinetic analysis with TACs of target and reference regions, so it is not affected by the error of estimated  $T_{\text{eq}}$ . On the other hand, the value of  $k'_3(t)$  in Equation (2) varies according to the concentration of bound raclopride, and estimates of  $BP_{\text{ND}}$  are considered to be an averaged value of specific binding over time, which is influenced by the dynamics of the free and bound raclopride. Despite this, in our simulation study of  $[^{11}\text{C}]$ raclopride, there was little difference between  $B^{\text{ref}}/F^{\text{ref}}$  and  $BP_{\text{ND}}$  estimated by the SRTM, and both had a linear correlation with  $B^{\text{ref}}$  (Figure 2). However,  $B^{\text{ref}}/F^{\text{ref}}$  became smaller than  $BP_{\text{ND}}$  and deviated from the linear relationship between  $B^{\text{ref}}/F^{\text{ref}}$  and  $B^{\text{ref}}$  in the region with low  $B^{\text{ref}}$  (Figure 2), especially for the TACs with high  $B_{\max}$ . This may be a result of imperfect attainment of the transient equilibrium within the 50 mins scan duration for the TAC with high binding. There was little effect of the error of  $B^{\text{ref}}$  for the graphical analysis, in which  $B^{\text{ref}}$  varied widely among three injections, whereas the error of  $B^{\text{ref}}/F^{\text{ref}}$